Integration of multi-source geophysical and geological data in a three-dimensional a-priori seismic velocity model for the Emilia-Romagna region

M. Abyat, C. Totaro, B. Orecchio, D. Presti, S. Scolaro

University of Messina, Department of Mathematical, Informatics, Physical and Earth Sciences (MIFT), Messina, Italy

The 2012 Emilia-Romagna seismic sequence mainly affected the central sector of the Ferrara arc and was characterised by the 20 May (Mw 6.1) and 29 May 2012 (Mw 6.0) mainshocks, followed by an extensive aftershock sequence associated with blind thrust systems buried beneath the Po Plain. Previous investigations have shown that this sequence illuminates the structural complexity of the Apennines foreland, revealing the activation of adjacent thrust segments and pronounced lateral heterogeneity along the Ferrara arc (Carannante et al., 2015; Govoni et al., 2014; Chiarabba et al., 2014). The dense permanent and temporary seismic networks deployed during the emergency phase generated a unique dataset for constraining crustal-scale physical models in northern Italy.

In this context, we present a new three-dimensional a-priori P-wave velocity model for the Emilia–Romagna region (10–13°E, 44–46°N), discretised on a 15 km × 15 km horizontal grid with a vertical spacing of 3 km. The model is developed through an integrated workflow in which velocity–depth functions are defined at each grid node and lateral consistency is imposed by spatial smoothing. Multiple independent datasets are incorporated, including Vp constraints from the three-dimensional Po Basin velocity model (Molinari et al., 2015), geological cross-sections from the ER3D structural model (Klin et al., 2019), regional-scale crustal and lithospheric information from published tomographic models (Di Stefano et al., 2020; Pezzo et al., 2018) and from the recent adjoint tomography of the Italian lithosphere (Magnoni et al., 2022), as well as seismogenic constraints derived from analyses of the 2012 sequence (Govoni et al., 2014). The integration of these heterogeneous data results in a geologically consistent three-dimensional starting model that explicitly accounts for the strong lateral velocity contrasts characteristic of the Po Plain, improving upon simplified one-dimensional or weakly constrained three-dimensional initial models.

The resulting model (defined as a-priori model) is intended to be employed as the initial velocity structure for future three-dimensional travel-time tomography of the Emilia region. High-quality P- and S-wave arrival times recorded by the seismic network operating during the 2012 sequence provide favourable ray coverage, particularly in the upper and middle crust, and are expected to support a stable inversion in the presence of strong lateral velocity contrasts and heterogeneous station spacing.

This work aims to contribute to the development of a robust seismic imaging framework for the Po Plain. Such an approach is expected to enhance the resolution of lateral heterogeneities within the sedimentary basin and improve constraints on the geometry of buried thrust systems, with implications for seismic hazard assessment in one of the most densely populated and industrialised regions of northern Italy.

References

Carannante S., Argnani A., Massa M., D'Alema E., Lovati S., Moretti M., Cattaneo M., Augliera P.; 2015. The May 20 (MW 6.1) and 29 (MW 6.0), 2012, Emilia (Po Plain, northern Italy) earthquakes: New seismotectonic implications from subsurface geology and high-quality hypocenter location. Tectonophysics, 655, 107-123.

Govoni A., Marchetti A., De Gori P., Di Bona M., Lucente F.P., Improta L., Chiarabba C., Nardi A., Margheriti L., Agostinetti N.P., Di Giovambattista R.; 2014. The 2012 Emilia seismic sequence (Northern Italy): Imaging the thrust fault system by accurate aftershock location. *Tectonophysics*, *622*, 44-55.

Chiarabba C., De Gori P., Improta L., Lucente F.P., Moretti M., Govoni A., Di Bona M., Margheriti L., Marchetti A., Nardi A.; 2014. Frontal compression along the Apennines thrust system: The Emilia 2012 example from seismicity to crustal structure. *Journal of Geodynamics*, *82*, 98-109.

Molinari I., Argnani A., Morelli A., Basini P.; 2015. Development and testing of a 3D seismic velocity model of the Po Plain sedimentary basin, Italy. *Bulletin of the Seismological Society of America*, *105*(2A), 753-764.

Klin P., Laurenzano G., Romano M. A., Priolo E., Martelli L.; 2019. ER3D: a structural and geophysical 3-D model of central Emilia-Romagna (northern Italy) for numerical simulation of earthquake ground motion. *Solid earth*, *10*(3), 931-949.

Di Stefano R., Ciaccio M. G.; 2020. Seismic Velocity Model of P- and S-waves for the Italian Lithosphere (1.0) [Data set]. Zenodo. https://doi.org/10.13127/tomorama.1

Pezzo G., De Gori P., Lucente F. P., Chiarabba C.; 2018. Pore pressure pulse drove the 2012 Emilia (Italy) series of earthquakes. *Geophysical Research Letters*, *45*(2), 682-690.

Magnoni F., Casarotti E., Komatitsch D., Di Stefano R., Ciaccio M.G., Tape C., Melini D., Michelini A., Piersanti A., Tromp, J.; 2022. Adjoint tomography of the Italian lithosphere. *Communications Earth & Environment*, *3*(1), 69.

Corresponding author: majed.abyat7@gmail.com

Constraining magma pressurization history at Mt. Etna volcano through geophysical observations and thermomechanical modeling

M. Bensing[1], S. Vinciguerra[1], G. Puglisi[2] & L. De Siena[3]

[1]*Dipartimento di Scienze della Terra, Università di Torino*
[2]*Istituto Nazionale di Geofisica e Vulcanologia, Sezione di Catania*
[3]*Dipartimento di Fisica e Astronomia, Università di Bologna*

Mt. Etna volcano lies on the northeastern coast of Sicily in the central Mediterranean and is one of the most active and hazardous stratovolcanoes in the world. Its southeastern flank is gradually sliding toward the Ionian Sea, a movement driven by gravitational spreading and tectonic forces that can be accelerated by magma pressurization. The volcano consists of a basaltic upper layer, 2-3 km in thickness, that overlies a 25-30 km thick carbonate basement, with sub-Etnean clays forming the uppermost part of the basement sequence (Bakker et al., 2019). The Pernicana fault in the north and three fault systems in the south, Mascalucia-Tremestieri, Fiandaca-Pennisi and Gravina, tectonically decouple Etna's southeastern flank from the rest of the volcanic edifice (Murray & de Vries, 2022), with stronger deformation patterns observed near Pernicana than in the southern fault systems (Pezzo et al., 2023; Murray & de Vries, 2022). Seismic tomography studies have revealed that a large intrusive body, indicated by a high P-wave velocity volume, exists in the center of the volcano (Giampiccolo et al., 2020; Díaz-Moreno et al., 2018; Alparone et al., 2012). Moreover, a low P-wave velocity and high Vp/Vs volume recorded below the eastern flank suggests the presence of fluid-filled fracture zones (Giampiccolo et al., 2020), which contribute to the flank's instability (Mattia et al., 2015).

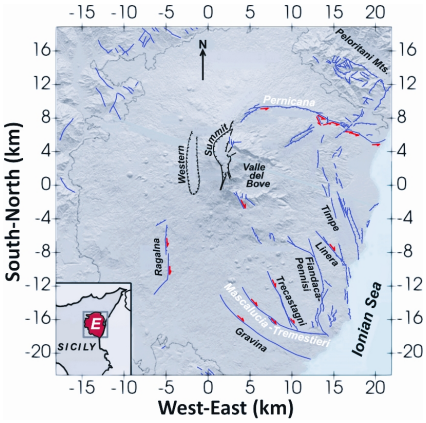

Fig. 1. Geological map of Mt. Etna volcano with main fault systems and structural features, modified from Murray and de Vries (2022). Blue lines indicate faults; those with ticks on the side represent downward movement, and those with red arrows display the direction of movement along strike-slip faults. Black lines show the bounding faults of the Summit graben and dashed lines the lateral extension of the Western Graben.

To simulate ground deformation, we used the code of LaMEM (Lithosphere and Mantle Evolution Model), which employs a staggered-grid finite difference method with a continuum Eulerian approach (Kaus et al., 2016). We constructed the 3D model geometry using the GeophysicalModelGenerator.jl package and real topographic data, all implemented in the Julia programming language (Kaus et al., 2024). Geological structures were defined based on geological maps and seismic velocity models, with rock properties assigned from laboratory measurements and typical upscaled values used in geodynamic simulations. The model focuses on a brittle upper crust and a southeastern flank that is mechanically decoupled from surrounding structures by weak rock zones. In total, five model geometries (Fig. 2 shows the simplest geometry version) and three rheology regimes with significant variation for shear modulus, cohesion and friction angle values were tested, revealing best fits for the least rigid model configurations. Furthermore, the implementation of a sub-vertical intrusive body and a spherical fluid reservoir showed considerable improvement compared to the simpler model geometry.

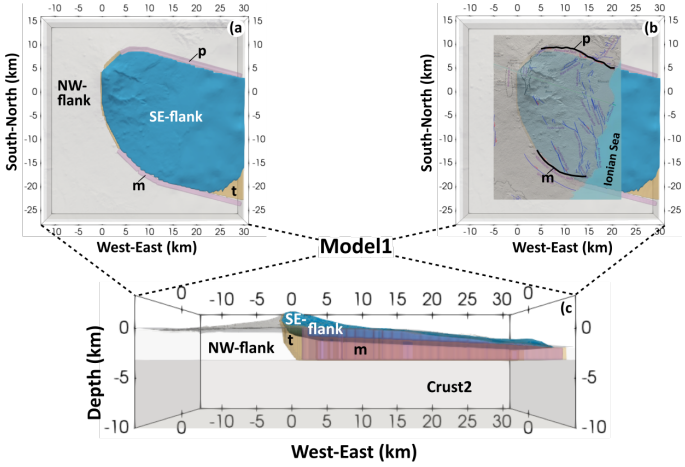

Fig. 2. Model1 geometry. t = thrust fault of Apennine-Maghrebian, m = Mascalucia-Tremestieri fault, p = Pernicana fault. (a) Horizontal view of the model domain and (b) visualization with a geological map from Murray and de Vries (2022). Black lines indicate the location of the Pernicana and Mascalucia-Tremestieri faults. (c) W-E vertical side view of the model domain that faces the volcano's southern side.

Our current modeling efforts focus on introducing magmatic activity and improving alignment with seismic and GPS observations from 2018 at the volcano. Giampiccolo et al. (2020) utilized time-lapse seismic imaging to reveal transient velocity changes during the December 2018 eruptive episode. Their findings showed a localized reduction in Vp and an associated increase in Vp/Vs within a shallow intruded dike below the upper southeastern flank, which indicated magma pressurization and culminated in an eruptive fissure striking NW-SE. Simultaneously a relative increase in Vp in the surrounding host rock was observed, marking stress propagation on the unstable flank. Deformation occurring on the lower end of the edifice was associated with another deeper and larger dike (between 1 and 5 km depth), which propagated roughly northsouthward (Mattia et al., 2020; De Novellis et al. 2019; Bonforte et al., 2019). Mattia et al. (2020) proposed a centrally located magma source that continued staying pressurized throughout and after the eruptive event in December 2018. Within the framework of our study, we would like to connect the main magmatic features of this period, and incorporate them into a time-dependent geodynamic model (see Fig. 3).

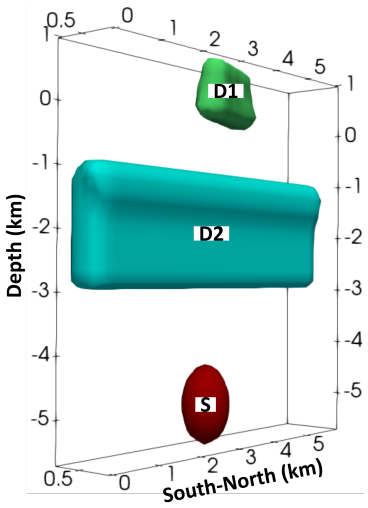

Fig. 3. Schematic representation of the magmatic system implemented in the geodynamic model for the December 2018 Etna eruption. The shallow dike (D1) represents intrusion beneath the upper southeastern flank. The deeper and larger dike (D2) accounts for deformation observed on the lower edifice and propagates north-south. The magma source (S) is centrally located.

References

Alparone, S., Barberi, G., Cocina, O., Giampiccolo, E., Musumeci, C., & Patanè, D. (2012). Intrusive mechanism of the 2008–2009 mt. etna eruption: Constraints by tomographic images and stress tensor analysis. *Journal of volcanology and geothermal research, 229*, 50–63. https://doi.org/10.1016/j.jvolgeores.2012.04.001.

Bakker, R. R., Violay, M. E., Vinciguerra, S., Fazio, M., & Benson, P. M. (2019). Constitutive laws for etnean basement and edifice lithologies. *Journal of Geophysical Research: Solid Earth, 124* (10), 10074–10088. https://doi.org/10.1029/2019JB017399.

Bonforte, A., Guglielmino, F., & Puglisi, G. (2019). Large dyke intrusion and small eruption: The december 24, 2018 mt. etna eruption imaged by sentinel-1 data. *Terra Nova, 31* (4), 405–412. https://doi.org/10.1111/ter.12403.

De Novellis, V., Atzori, S., De Luca, C., Manzo, M., Valerio, E., Bonano, M., . . .others (2019). Dinsar analysis and analytical modeling of mount etna displacements: The december 2018 volcano-tectonic crisis. *Geophysical Research Letters, 46* (11), 5817–5827. https://doi.org/10.1029/2019GL082467.

Díaz-Moreno, A., Barberi, G., Cocina, O., Koulakov, I., Scarfi, L., Zuccarello, L., . . . others (2018). New insights on mt. etna's crust and relationship with the regional tectonic framework from joint active and passive p-wave seismic tomography. *Surveys in geophysics, 39* , 57–97. https://doi.org/10.1007/s10712-017-9425-3.

Giampiccolo, E., Cocina, O., De Gori, P., & Chiarabba, C. (2020). Dyke intrusion and stress-induced collapse of volcano flanks: The example of the 2018 event at mt. etna (sicily, italy). *Scientific reports, 10* (1), 6373. https://doi.org/10.1038/s41598-020-63371-3.

Kaus, B. J., Popov, A. A., Baumann, T., Pusok, A., Bauville, A., Fernandez, N., & Collignon, M. (2016). Forward and inverse modelling of lithospheric deformation on geological timescales. In *Proceedings of nic symposium* (Vol. 48, pp. 978–983). http://hdl.handle.net/2128/9842.

Kaus, B. J., Thielmann, M., Aellig, P., de Montserrat, A., de Siena, L., Frasukiewicz, J., . . . others (2024). Geophysicalmodelgenerator. jl: A julia package to visualise geoscientific data and create numerical model setups. *Journal of Open Source Software, 9* (103), 6763. https://doi.org/10.21105/joss.06763.

Mattia, M., Bruno, V., Caltabiano, T., Cannata, A., Cannavo, F., D'Alessandro, W., . . . others (2015). A comprehensive interpretative model of slow slip events on mt. etna's eastern flank. Geochemistry, Geophysics, Geosystems, 16 (3), 635–658. https://doi.org/10.1002/2014GC005585.

Mattia, M., Bruno, V., Montgomery-Brown, E., Patanè, D., Barberi, G., & Coltelli, M. (2020). Combined seismic and geodetic analysis before, during, and after the 2018 mount etna eruption. *Geochemistry, Geophysics, Geosystems, 21* (9), e2020GC009218. https://doi.org/10.1029/2020GC009218.

Murray, J. B., & de Vries, B. v. W. (2022). Basement sliding and the formation of fault systems on mt. etna volcano. *Journal of Volcanology and Geothermal Research, 428* , 107573. https://doi.org/10.1016/j.jvolgeores.2022.107573.

Pezzo, G., Palano, M., Beccaro, L., Tolomei, C., Albano, M., Atzori, S., & Chiarabba, C. (2023). Coupling flank collapse and magma dynamics on stratovolcanoes: the mt. etna example from insar and gnss observations. *Remote Sensing, 15* (3), 847.

https://doi.org/10.3390/rs15030847.

Corresponding author: michelle.bensing@unito.it

A Numerical Approach to Investigate a New Style of Volcanotectonic Deformation: Dyke-induced Antithetic Faulting

S. Brando[1], F. L. Bonali[1,2], A. Luppino[1], F. Pasquaré Mariotto[3], A. Tibaldi[1,2]

[1] Department of Earth and Environmental Sciences, University of Milan-Bicocca, Milan, Italy
[2] CRUST – Interuniversity Centre for 3D Seismotectonics with Territorial Applications, Chieti, Italy
[3] Department of Human and Innovation Sciences, Insubria University, Como, Italy

Surface brittle deformation in volcano-tectonic environments provides key insights into magma intrusion processes at shallow crustal levels. Dyke intrusions, even when arrested at depth, can transfer stresses toward the surface and induce faults and graben structures (Gudmundsson et al., 1999). However, the mechanical controls governing fault asymmetry and surface deformation patterns remain incompletely understood.

This study primarily focuses on numerical modelling to investigate the role of dyke geometry and rheological contrasts in controlling dyke-induced surface deformation. The modelling approach is inspired by field observations from a subglacial volcanic cone in the Northern Volcanic Zone of Iceland, characterised by a strongly asymmetric summit graben (fig. 1).

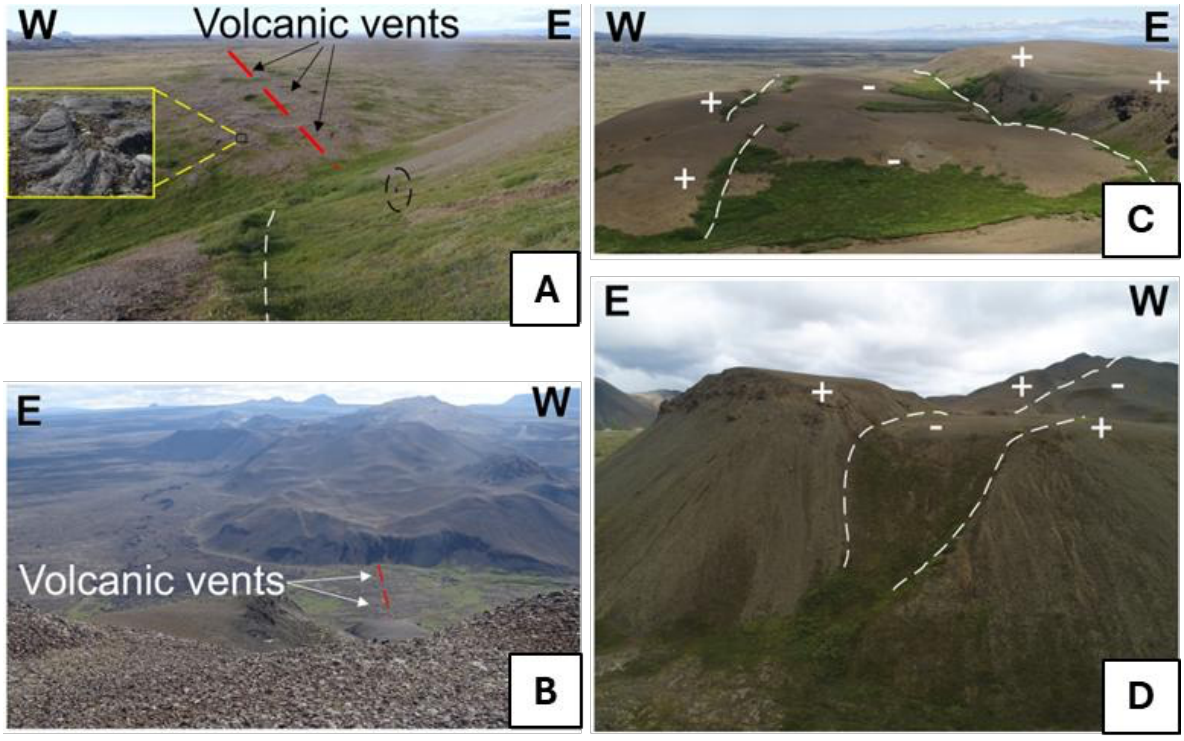

Figure 1. Field photographs showing eruptive fissures at the northern and southern terminations of the ridge (A–B) and the associated summit graben, illustrated in plan view (C) and in section along the northern flank (D).

A suite of 2D numerical models was developed using the Finite Element Method (FEM) implemented in COMSOL Multiphysics to simulate the elastic response of the crust to dyke intrusion. Although simplified, the elastic assumption is appropriate for modelling the early stages of crustal response to magmatic overpressure and is widely adopted in the literature (Pollard et al., 1983; Gudmundsson et al., 2007; Drymoni et al., 2020, 2021; Tibaldi et al., 2022; Bonali et al., 2024).

Several modelling scenarios, supported by previous field data collected, were explored to test the relationships between surface graben development and key controlling parameters, including dyke geometry and depth, rheological layering of the host rocks, surface topography and interaction with pre-existing tectonic structures at depth (fig. 2).

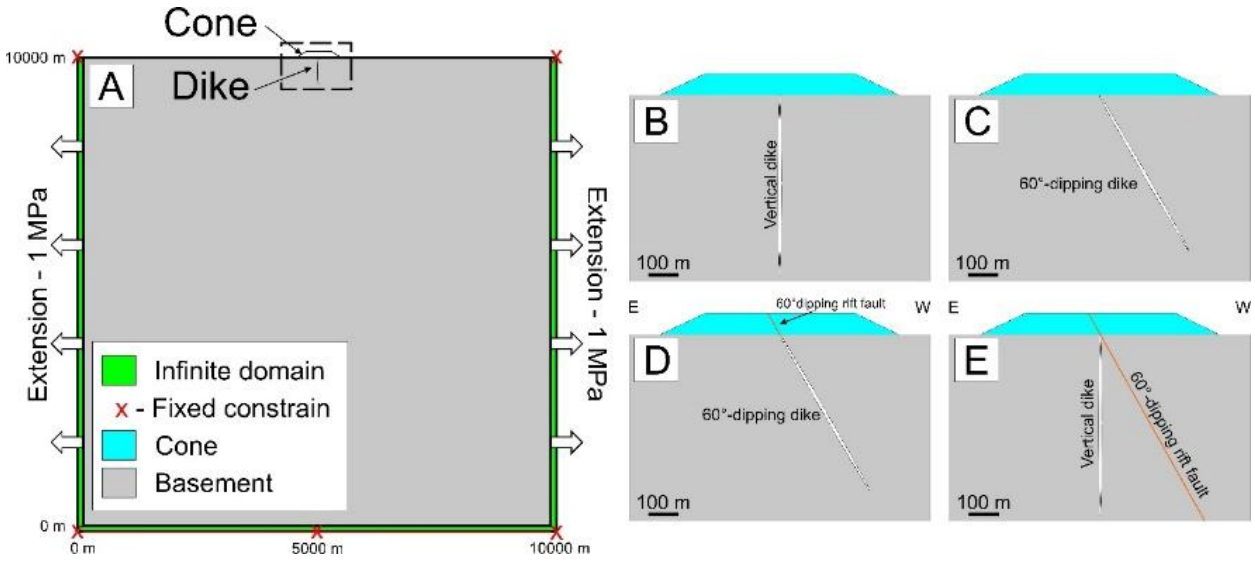

Figure 2. A) Numerical models setup; B) vertical dyke; C) 60°-dipping dyke D) 60°-dipping dyke intruding a 60°-dipping border fault affecting the cone; and (E) vertical dyke interacting with a 60°-dipping border fault.

Model outputs include tensile stress, von Mises stress and principal stress orientations (σ_1 and σ_3), allowing assessment of conditions favourable to tensile fracturing and shear failure. Results show that models incorporating a marked rheological contrast and an inclined dyke generate a strongly asymmetric stress field at the surface, with higher tensile and von Mises stresses concentrated on one side of the graben. This configuration reproduces the observed asymmetry in fault offsets and promotes preferential localisation of deformation above the weaker volcanic edifice. In addition, the rheological contrast significantly reduces tensile stresses above the dyke tip, favouring dyke arrest within the cone rather than surface eruption (fig. 3).

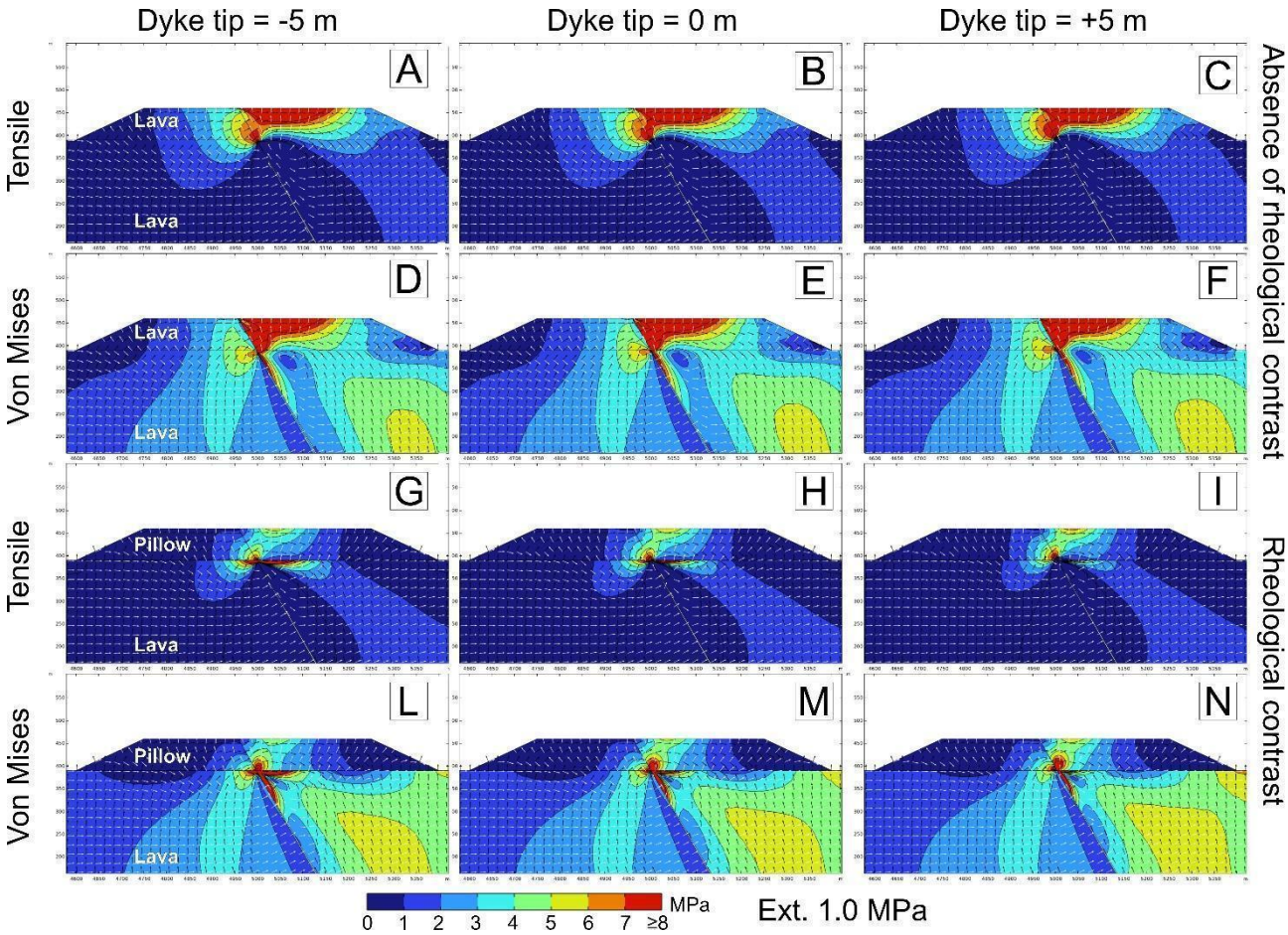

Figure 3. Numerical results for models with an inclined (60° west-dipping) dyke connected to a pre-existing normal fault, tested under two rheological conditions: (A–F) uniform stiffness ratio (1:1) and (G–N) strong mechanical contrast (1:10) between the cone and the substratum. Each triplet of panels shows tensile (A–C, G–I) and von Mises (D–F, L–N) stress distributions for dyke tips located 5 m below the cone base, at the cone base, and 5 m above the cone base (intruding the pillow cone). All models were subjected to an extensional stress field of 1 MPa and a dyke overpressure of 4 MPa; σ_1 is represented by white arrows, and σ_3 by black ones.

These findings highlight the important role of numerical modelling in exploring the combined effects of dyke geometry, mechanical layering and pre-existing faults on volcano-tectonic deformation. They suggest that asymmetric graben development and dyke arrest are likely common outcomes in volcanic systems characterized by strong rheological contrasts and inherited structures, with important implications for interpreting surface deformation and assessing volcanic unrest.

References

Bonali, F. L., Brando, S., Pasquaré Mariotto, F., Luppino, A., & Tibaldi, A. Magmatically driven antithetic faulting: structural and numerical insights. Journal of Structural Geology, under review.

Bonali, F. L., Corti, N., Pasquaré Mariotto, F., De Beni, E., Bressan, S., Cantarero, M., Russo, E., Neri, M., & Tibaldi, A. (2024). 3D study of dyke-induced asymmetric graben: The 1971 Mt. Etna (Italy) case by structural data and numerical modelling. Journal of Structural Geology, 187, 105231. https://doi.org/10.1016/j.jsg.2024.105231

Drymoni, K., Browning, J., & Gudmundsson, A. (2020). Dyke-arrest scenarios in extensional regimes: Insights from field observations and numerical models, Santorini, Greece. Journal of Volcanology and Geothermal Research, 396, 106854. https://doi.org/10.1016/j.jvolgeores.2020.106854

Drymoni, K., Browning, J., & Gudmundsson, A. (2021). Volcanotectonic interactions between inclined sheets, dykes, and faults at the Santorini Volcano, Greece. Journal of Volcanology and Geothermal Research, 416, 107294. https://doi.org/10.1016/j.jvolgeores.2021.107294

Gudmundsson, A. (2007). Conceptual and numerical models of ring-fault formation. Journal of Volcanology and Geothermal Research, 164(3), 142-160.

Gudmundsson, A., Marinoni, L. B., & Martí, J. (1999). Injection and arrest of dykes: Implications for volcanic hazards. Journal of Volcanology and Geothermal Research, 88(1–2), 1–13. https://doi.org/10.1016/S0377 0273(98)00107-3

Pollard, D. D., Delaney, P. T., Duffield, W. A., Endo, E. T., & Okamura, A. T. (1983). Surface deformation in volcanic rift zones. In P. Morgan & B. H. Baker (Eds.), Developments in Geotectonics (Vol. 19, pp. 541–584). Elsevier. https://doi.org/10.1016/B978-0-444-42198-2.50036-5

Tibaldi, A., Bonali, F. L., Corti, N., Russo, E., Drymoni, K., De Beni, E., Branca, S., Neri, M., Cantarero, M., & Pasquarè Mariotto, F. (2022). Surface deformation during the 1928 fissure eruption of Mt. Etna (Italy): Insights from field data and FEM numerical modelling. Tectonophysics, 837, 229468. https://doi.org/10.1016/j.tecto.2022.229468

Corresponding author: sofia.brando@unimib.it

Long-Range Acoustic and Seismic Effects of the 1920 Vergiate Explosion: Insights from Physical Modeling for a Century-Old Event

R. Console[1,2], G. Mele[2]

[1] *Center of Integrated Geomorphology for the Mediterranean Area, Potenza*
[2] *Istituto Nazionale di Geofisica e Vulcanologia, Roma*

On 26 November 1920, a major industrial explosion at the Officine Elettrochimiche Dr. Rossi in Vergiate, northern Italy, generated powerful acoustic and seismic waves that were observed and recorded over a wide portion of Italy and neighboring regions. Occurring in a period marked by strong geophysical institutions but declining post–World War I scientific investment, the event became the subject of a detailed investigation by Italian geophysicist Emilio Oddone, commissioned by the Central Office of Meteorology and Geodynamics. Oddone's work combined instrumental seismographic records with an exceptional collection of more than two hundred eyewitness reports, making the Vergiate explosion one of the best-documented non-natural energetic events of the early twentieth century.

This contribution revisits Oddone's analysis from a modern geophysical perspective, focusing on the integration of historical data with contemporary physical models of seismic and acoustic wave propagation. We reassess both atmospheric sound propagation and seismic observations in light of contemporary theoretical and observational advances. We contextualize early interpretations of long-range acoustic phenomena within the scientific knowledge available at the time and compare them with modern models that explicitly incorporate atmospheric stratification and upper-atmosphere layers, such as the ozone layer and the thermosphere, whose roles in sound ducting and refraction were only recognized decades later. Particular attention is devoted to the "silent zone" reported at intermediate distances from the source, as well as to the anomalous audibility observed farther away, phenomena that today can be more consistently explained within a layered-atmosphere framework. Applying these propagation modes to Oddone's (1921) observations, the acoustic pattern of the Vergiate explosion can be interpreted as a sequence of arrivals: direct waves near the source, up to several tens of kilometers; a first silent zone between roughly 60 and 100 km; stratospheric arrivals extending up to 150–200 km; a second silent zone; and a second stratospheric bounce arriving beyond 300 km.

On the seismic side, we reanalyze the records collected by Oddone from six stations and provide the first quantitative estimate of the local magnitude of the Vergiate explosion, obtaining $M_L = 3.45 \pm 0.30$. This estimate is compared with modern events using integrated datasets from global seismic and infrasound networks, demonstrating the potential of combined observational-modeling approaches for understanding both historical and contemporary explosive events.

The most notable comparison is with the 4 August 2020 Beirut port disaster. The Beirut event was recorded by multiple seismic and infrasound stations belonging to the global network established to monitor compliance with the Comprehensive Nuclear-Test-Ban Treaty (CTBT), with infrasound detections extending up to approximately 6,000 km from the source. Using these data, previous studies estimated magnitudes of mb = 3.6 and Mw = 3.3, placing the Vergiate explosion in a comparable energetic range despite the radically different observational capabilities available a century earlier.

During the preparation of this study, an accidental explosion occurred on 9 December 2024 at the ENI fuel depot in Calenzano, central Italy. Although a local magnitude of only 0.9 was reported, the accident resulted in several fatalities and attracted widespread media attention, highlighting once again the societal impact of industrial explosions even at relatively small seismic magnitudes.

By integrating historical documentation, observational records, and physical models, this study emphasizes the enduring scientific value of early observational datasets and illustrates how interpretations of complex wave phenomena evolve alongside advances in theory, instrumentation, and global monitoring infrastructures. Despite this significance, the Vergiate explosion remains largely absent from contemporary reference compilations, including widely used public databases of ammonium nitrate–related incidents. Recovering and reassessing this case not only contributes to the history of seismology and atmospheric acoustics but also provides a long-term perspective on the monitoring and interpretation of large anthropogenic explosions.

Corresponding author: giuliana.mele@ingv.it

Calibration of the Local Magnitude Scale (M_L) for Eastern Cuba

Eduardo R. Diez Zaldívar [1], Denis Sandron [1], Manuel Cutie Mustelier [2]

[1] Istituto Nazionale di Oceanografia e di Geofisica Sperimentale –OGS Centro di Ricerche Sismologiche, Italy
[2] Centro Nacional de Investigaciones Sismologicas - CENAIS

In this study, we developed a local magnitude scale for the southeastern region of Cuba, the part of the island exposed to the greatest seismic hazard due to its proximity to the Oriente fault system.
From the 2011-2021 Cuban catalogue, 7750 earthquakes with $M_L > 2$ were selected, distributed in the region 19-22N; 73-79W and recorded by at least 4 seismic stations (of the Cuban CW network) within 500 km of the hypocentre. The resulting input data set includes 33916 amplitude measurements of the horizontal components.
The new formula for the local magnitude M_L is defined as follows:

$$\boldsymbol{M_L = log_{10}(A) + 1.000 log_{10}(R) + 0.003R - 1.963}$$

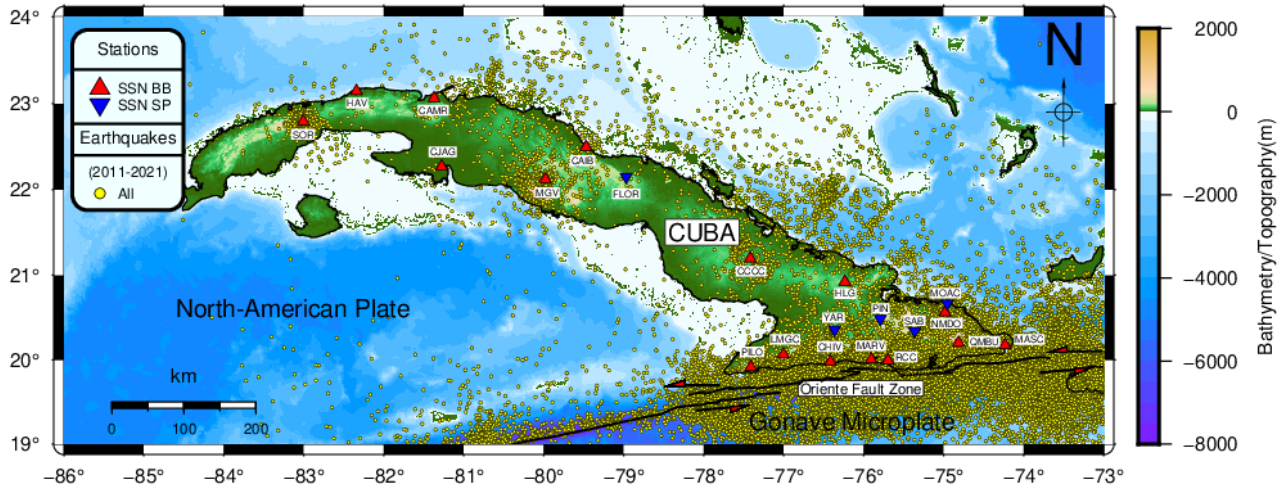

Fig. 1 – *The Cuba island in the Caribbean tectonic context. The main fault systems (black lines; red arrows represent the fault relative movement), with the Bartlett-Cayman fault system (Oriente) and other relevant fault systems in the region.*

In our study, we determined the values of the coefficients of the ML equation based on Ritcher's original definition and chose 17 km as the anchor point according to Hutton and Boore (1987). The local attenuation curve or distance correction for southeastern Cuba was estimated by linear regression analysis procedure using the measured horizontal components amplitudes (33,916).
This calculation provided values for the empirical coefficients for geometrical spreading and anelastic attenuation that control the amplitude–distance correction curve.

The curve found is slightly less attenuated than that previously defined for this area by Moreno (2002) and lies in between that and the curve obtained for California by Hutton and Boore (1987). The correction values found for the stations are consistent with the local geology.

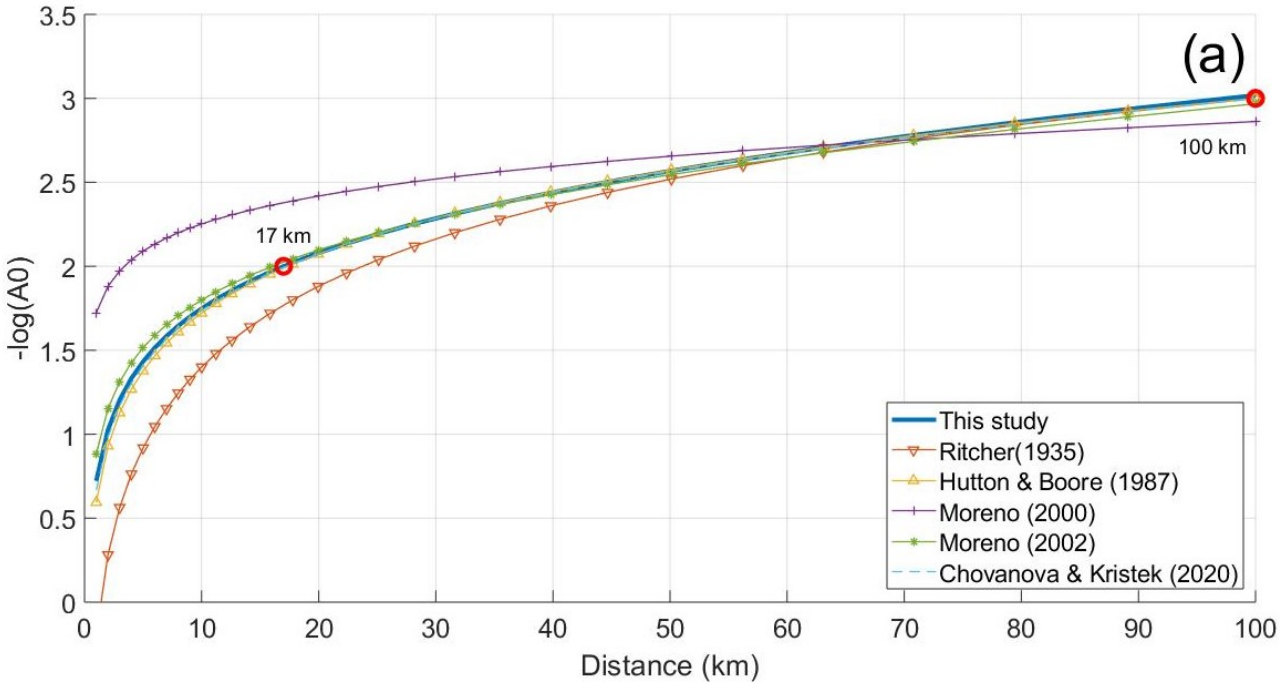

Fig. 2 – Comparison of attenuation curves between this study and Ritcher (1935), Hutton & Boore (1987) and Moreno (2000, 2002)..

Acknowledgments

The authors would like to express their gratitude to Enrico Priolo for his help in the mathematical algorithms understanding and programming

References

CENAIS (2023). Catálogo de terremotos (extracción parcial de los años 2011 al 2021 del catálogo general de terremotos), Fondos del CENAIS (in Spanish).

Chovanová, Z., and J. Kristek (2018). A local magnitude scale for Slovakia, Central Europe, Bull. Seismol. Soc. Am. 108, 5A, 2756–2763, doi: 10.1785/0120180059.

Diez Zaldívar E. R., M. C. Mustelier, C. M. Moracén, R. P. Cláres, V. Poveda Brossard, Z. Yinxing, C. Yang, and W. Fengxia (2014). Modernización de la red sísmica cubana, Instalación, calibración y puesta a punto, Rev. Fac. Ing. UCV 29, 69–78 (in Spanish).

Hutton, L. K., and D. M. Boore (1987). The ML scale in southern California, Bull. Seismol. Soc. Am. 77, 2074–2094, doi: 10.1785/ BSSA0770062074.

Richter, C. F. (1935). An instrumental earthquake magnitude scale, Bull. Seismol. Soc. Am. 25, no. 1, 1–32.

Corresponding author: ediezzaldivar@ogs.it

Characterisation of continuous gravity signals from four gravimeters of the Italian Fiducial Gravimetric Network

N. Dottore[1], F. Greco[1], G. Berrino[1], F. Riguzzi[1], D. Sampietro[1,2], D. Carbone[1], D. Contrafatto[1], A. Messina[1], L.T. Mirabella[1], G. Ricciardi[1], A. Fedele[1], I. Fiori[3], V. Dattilo[3], L. Lunghini[3], C. Giunchi[1], M. Olivieri[1], F. Sanseverino[1], M. Crespi[1,4,5,6], F. Sansò[1,2,6], D. Accardo[7], A. Di Ruocco[7], P. Franzese[7]

[1] *Istituto Nazionale di Geofisica e Vulcanologia (INGV)*
[2] *GReD s.r.l.*
[3] *European Gravitational Observatory*
[4] *Geodesy and Geomatics Division-DICEA, Sapienza University of Rome*
[5] *Sapienza School for Advanced Studies, Sapienza University of Rome*
[6] *National Academy of the Lincei*
[7] *Centre for Advance Metrological and Technology Services (CeSMA), Università degli Studi di Napoli "Federico II"*

INGV is currently developing the Italian Fiducial Gravimetric Network, which will comprise approximately ten stations evenly distributed across the national territory (Fig. 1). The network will comprise several INGV stations, equipped with superconducting or absolute (Quantum and Ballistic) gravimeters, the only instruments capable of providing high-precision and stable measurements over long periods, operating in continuous or quasi-continuous mode. The primary aim of the network is to monitor long-term and long-wavelength variations of the gravitational field over the Italian territory. This network supports the newly established National Reference Gravimetric (G0) and Height (H0) Network (Barzaghi et al., 2026). Four stations of the network managed by INGV — Cascina, Napoli, Sos Enattos and Nicolosi — are already operational and acquiring data.

Fig. 1 – Map of the stations in the Italian Fiducial Gravimetric Network.

Among these four stations, two are equipped with superconducting relative gravimeters (iGravs, manufactured by GWR Instruments): iGrav#25 and iGrav#70 were installed at Nicolosi and Sos Enattos, respectively (Figs. 2a e 2b). The Nicolosi station, operational since 2016, is of particular interest for the monitoring of Mt. Etna volcano. The Sos Enattos station, located at the Italian candidate site for the Einstein Telescope (the future European gravitational-wave observatory), was installed in September 2025 at a preliminary location and will be relocated to its final site in early 2026. In November and December 2025, two Absolute Quantum Gravimeters (AQGs manufactured by Exail) were deployed at Cascina (AQG-A09, installed at the EGO site, where the Virgo gravitational-wave detector is hosted; Fig. 3a) and Naples (AQG-B06, installed at the CeSMA, University of Naples “Federico II”; Fig. 3b). All stations are remotely controlled.

Fig. 2a – Nicolosi station (NIC). iGrav#25 superconducting gravimeter operational since 2016.

Fig. 2b – Sos Enattos station (NU). iGrav#70 superconducting gravimeter during a test in the Rimisa facility at the Sos Enattos Mine.

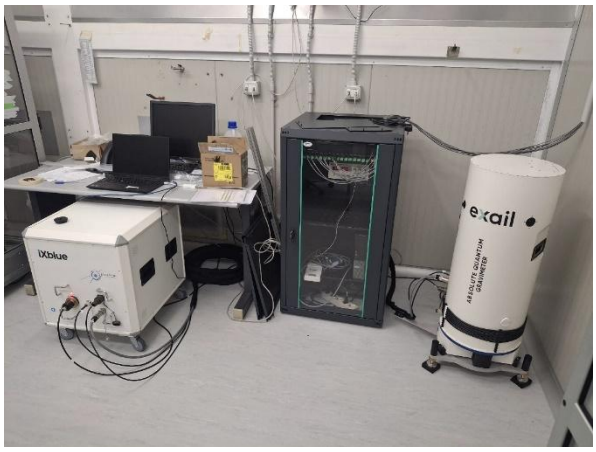

Fig. 3a – Cascina station (PI). AQG-A09 gravimeter in the clean room. On the left is the control unit and on the right is the sensor head.

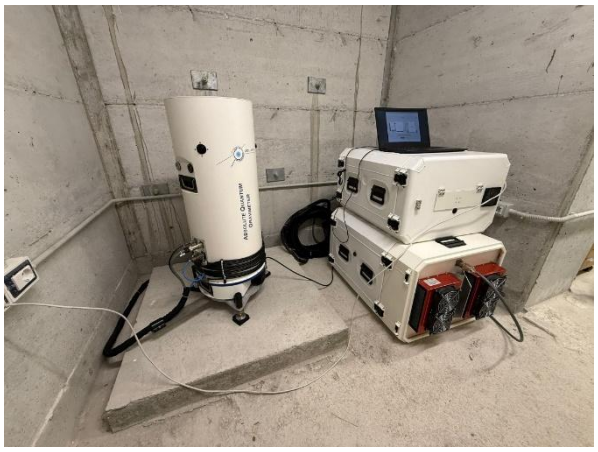

Fig. 3b – Napoli station (CeSMA). AQG-B06 gravimeter. On the left the sensor head and on the right the control units.

Since the installation of each gravimeter, daily analysis of the incoming signal has been carried out. Here we present preliminary results from the already available data.
In this first stage, the main objective has been to characterise the recorded signals, evaluating instrumental sensitivity and stability, as well as analysing the environmental noise. In the subsequent phase, the focus will move to the estimation and separation of local contributions from regional-scale signals. To this end, the sites have been or will be equipped with sensors for measuring key meteorological parameters and GNSS receivers to monitor ground deformations and, where possible, with piezometers to measure the oscillations of the local groundwater table.

Acknowledgments

AQG-B06 gravimeter was funded by INGV as part of the “GRINT” PIR 0013 Project in implementation of Action II.1 of the PON Research and Innovation 2014-2020.

AQG-A09 gravimeter was funded by the PNRR, “Sistema di Monitoraggio Integrato” (M2C4M1_I.1.1).

iGrav#70 superconducting gravimeter was funded by the PNRR project MEET (WP7 FABER).

iGrav#25 superconducting gravimeter was funded by the VULCAMED project, Ricerca & Competitività “2007-2013" (Cod. PONa3_00278/F).

References

Barzaghi et al.; 2026: The new reference gravity network in Italy. Bulletin of Geophysics and Oceanography, in publication.

Corresponding author: nancy.dottore@ingv.it

Multi-Technique analysis of Ocean Tides and Ocean Tidal Loading in the Northern Adriatic using GNSS PPP, Tide Gauges, and GNSS Reflectometry

A. Fantoni[1], C. Braitenberg[1], R. Devoti[2]

[1] *University of Trieste, Department of Mathematics, Informatics and Geosciences (MiGE), Italy*
[2] *Istituto Nazionale di Geofisica e Vulcanologia, Osservatorio Nazionale Terremoti, Rome, Italy.*

The northern Adriatic Sea constitutes a unique natural laboratory for the investigation of ocean tides and their geodetic and oceanographic consequences. Unlike most of the Mediterranean basin, which is characterized by microtidal conditions, the northern Adriatic exhibits the largest tidal ranges in the region, frequently exceeding 1 m during spring tides. This anomalous behaviour is primarily controlled by the basin's shallow bathymetry, wide continental shelf, elongated geometry, and semi-enclosed configuration, which together favor resonant amplification of both diurnal and semidiurnal tidal constituents (Janeković et al., 2005; Medvedev et al., 2020). In addition, the interaction between astronomical tides, basin-scale seiches, and meteorological forcing (e.g., Bora and Scirocco winds, atmospheric pressure variations) produces complex sea-level variability and extreme events such as "acqua alta", with significant societal and economic impacts along the densely populated coastline (Camuffo et al., 2023).

In this contribution, we present a comprehensive and multi-technique analysis of tidal dynamics and ocean tidal loading (OTL) in the northern Adriatic region, integrating tide gauge (TG) records, GNSS reflectometry (GNSS-R) and high-rate GNSS precise point positioning (PPP) solutions for crustal deformation (see Figure 1 for stations map distribution).

TG observations from multiple stations spanning the northern Adriatic confirm the progressive amplification of semidiurnal energy toward the head of the basin, with the principal lunar semidiurnal tide M_2 and the solar semidiurnal tide S_2 becoming increasingly dominant relative to the diurnal constituent K_1. Harmonic analysis of TG time series shows good overall agreement with the FES2014b global ocean tide model (Carrère et al., 2015), while also revealing localized discrepancies in amplitude and phase, particularly at stations characterized by complex coastal geometry and shallow-water dynamics, consistent with previous regional studies (Tsimplis et al., 1995; Martens et al., 2020).

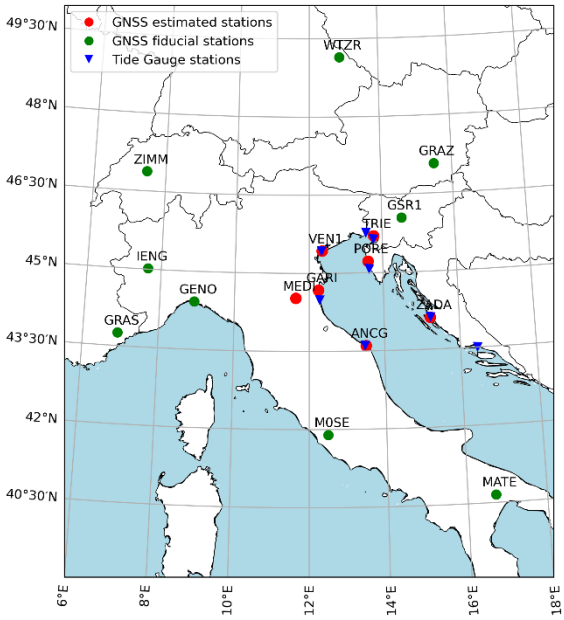

Fig. 1 - Distribution of the selected GNSS, GNSS-R and TG stations. The red dots represent the GNSS investigated stations, the green dots represent the network of fiducial stations, and the blue triangles represent the TG stations.

GNSS reflectometry is employed to extend sea-level observations to sites lacking conventional TGs. Sea surface height (SSH) time series derived from GNSS-R at several coastal stations along the northern Adriatic (VEN1, GARI, PORE, and an additional station located in Sistiana, close to Trieste) exhibit strong temporal coherence with nearby TG records, with correlation coefficients exceeding 90% (Figure 2).

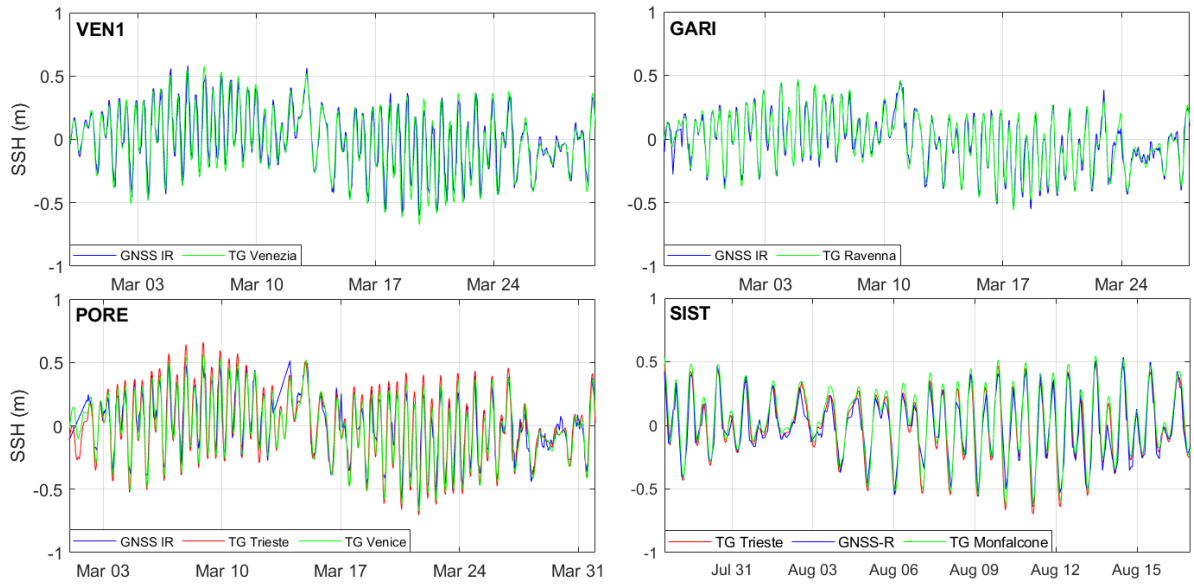

Fig. 2 - Comparison between GNSS-R derived SSH time series and TG measurements for the four northern Adriatic stations.

Spectral analyses demonstrate that both diurnal and semidiurnal tidal constituents are clearly resolved, with amplitude differences of only 2-3 cm relative to TG estimates. A dedicated case study at the Sistiana station further confirms the robustness of the technique, even under sub-optimal observational conditions such as limited azimuthal coverage and single-constellation GPS tracking. These results are consistent with recent applications of GNSS-R for coastal sea-level monitoring (Tabibi et al., 2020; Devoti et al., 2023) and highlight its potential as a cost-effective complement to traditional TG networks.

To investigate the solid Earth response to ocean tides, GNSS PPP solutions were analyzed to estimate three-dimensional OTL displacements at multiple stations surrounding the Adriatic basin. Modelled OTL displacements were computed using the FES2014b tide model and elastic Earth Green's functions and compared with GNSS-derived harmonic estimates. The vertical component (Figure 3) shows the clearest tidal signature, with the semidiurnal M_2constituent dominating the loading signal and exhibiting excellent agreement in both amplitude and phase between observations and model predictions.

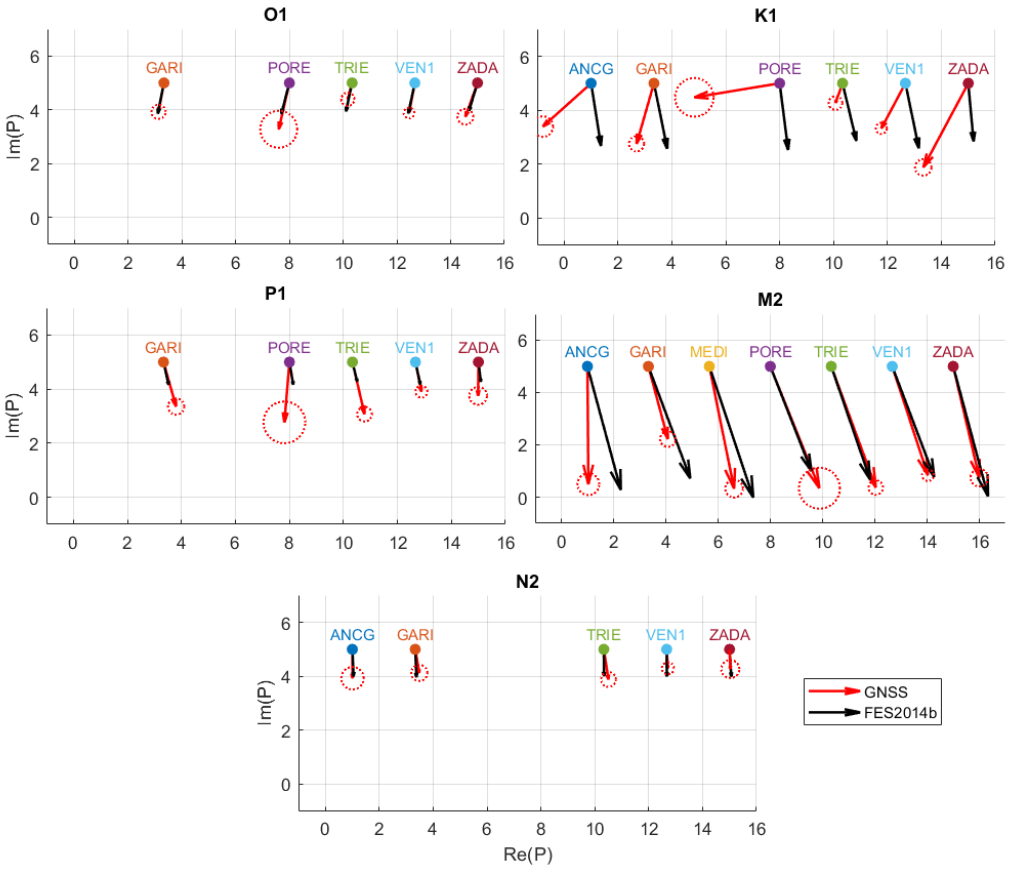

Fig. 3 - Phasor diagram showing the complex representation of the main OTL constituents in the northern Adriatic Sea. Each vector combines the amplitude and phase of the vertical loading displacement. Red arrows indicate estimates derived from harmonic analysis of GNSS time series, while black arrows represent predictions from the FES2014b OT model. The reference system is defined by standard Cartesian coordinate axes, with positive angles measured counterclockwise. Phasors are represented in the complex plane, with the real component along the horizontal axis and the imaginary component along the vertical axis.

The secondary semidiurnal component N_2 is also consistently resolved. Diurnal constituents, particularly K_1, display larger discrepancies, including amplitude inflation and phase offsets, which can be attributed to near resonance between the diurnal tidal period and the GNSS orbital repeat cycle, as well as residual orbit and multipath effects (King et al., 2006; Abbaszadeh et al., 2020). Horizontal OTL displacements further reveal a clear contrast between semidiurnal and diurnal behaviour. The M_2 horizontal response is spatially coherent and well aligned with model predictions, reflecting the propagation of the semidiurnal tide from the Otranto Strait toward the northern Adriatic. In contrast, horizontal K_1displacements show greater scatter and systematic amplitude biases, reinforcing the known limitations of GNSS for resolving diurnal loading signals.

Overall, this study provides the first GNSS-based OTL analysis in the northern Adriatic region performed at an hourly temporal resolution. The GNSS PPP solutions enable the direct observation of sub-daily elastic crustal responses to ocean tides in a shallow, semi-enclosed basin, representing a significant methodological advancement for the region. The consistency between GNSS-derived OTL signals, GNSS-R sea level estimates, and traditional TG observations demonstrates the robustness of the integrated approach and confirms the capability of GNSS techniques to resolve both oceanographic and geophysical tidal processes at unprecedented temporal detail. These results not only improve the understanding of tidal dynamics and loading in the northern Adriatic but also establish a new benchmark for future high-resolution GNSS studies of coastal ocean-solid Earth interactions, with important implications for sea level monitoring, geodetic reference frame stability, and coastal hazard assessment under ongoing climate change.

References

Abbaszadeh, M., King, M. A., Clarke, P. J., & Penna, N. T. (2020). Benefits of multi-GNSS for ocean tide loading displacement estimation. *Journal of Geophysical Research: Solid Earth, 125*(4), e2019JB018712.

Camuffo, D., Sturaro, G., & Malinverno, E. (2023). *A treatise on Venetian climate and acqua alta*. Springer.

Carrère, L., Lyard, F., Cancet, M., Guillot, A., & Picot, N. (2015). FES2014, a new tidal model—Validation results and perspectives for improvements. *Proceedings of the ESA Living Planet Symposium*.

Devoti, R., Rutigliano, P., & Pietrantonio, G. (2023). GNSS interferometric reflectometry for coastal sea-level monitoring in the Mediterranean. *Remote Sensing, 15*(3), 642. https://doi.org/10.3390/rs15030642

Janeković, I., Kuzmić, M., & Cushman-Roisin, B. (2005). Numerical simulation of tidal dynamics in the Adriatic Sea. *Journal of Geophysical Research: Oceans, 110*(C3), C03S19. https://doi.org/10.1029/2004JC002453

King, M. A., Penna, N. T., & Clarke, P. J. (2006). GPS-based tidal loading displacements and ocean tide models. *Geophysical Journal International, 166*(2), 787–802. https://doi.org/10.1111/j.1365-246X.2006.03037.x

Martens, H. R., et al. (2020). Comparison of global ocean tide models using GNSS loading observations. *Journal of Geophysical Research: Solid Earth, 125*(7), e2019JB018674.

Medvedev, I. P., Rabinovich, A. B., & Kulikov, E. A. (2020). Tidal resonance in the Adriatic Sea. *Ocean Science, 16*(4), 911–926. https://doi.org/10.5194/os-16-911-2020

Tabibi, S., van Dam, T., & Sneeuw, N. (2020). Tidal analysis using GNSS reflectometry. *Journal of Geophysical Research: Oceans, 125*(6), e2019JC015325. https://doi.org/10.1029/2019JC015325

Tsimplis, M. N., Proctor, R., & Flather, R. A. (1995). A two-dimensional tidal model for the Mediterranean Sea. *Journal of Geophysical Research: Oceans, 100*(C8), 16223–16239. https://doi.org/10.1029/95JC01671

Corresponding author: anna.fantoni@phd.units.it

Modelling the effects of gravitational instabilities on subduction zone initiation at passive margins

Valeria Fedeli[1], Alessandro Regorda[1], Anna Maria Marotta[1]

[1] *Università degli Studi di Milano, Dipartimento di Scienze della Terra "A. Desio"*

Subduction is a widely studied process, but the mechanisms leading to the initiation of a new subduction zone are poorly understood. Two main types of subduction zone initiation (SZI) are currently recognized: induced, when tectonic convergence is dominant, and spontaneous, when SZI is mainly driven by local forces, i.e., the negative buoyancy due to the gravitational instability of the plate (Stern 2004; Stern and Gerya 2018; Crameri et al. 2020). The passive margins are potential sites for spontaneous SZI due to the natural gravitational instabilities that characterize these geodynamic settings, caused by density, composition, strength and temperature lateral contrasts, topographic discontinuity, and sedimentary loading. These instabilities should favor the initiation of a new subduction zone (Stern and Gerya 2018; Lallemand and Arcay 2021; Arcay et al. 2020), but previous research suggests that these local forces are not strong enough to develop a self-sustained subduction and that the collapse of a passive margin without horizontal tectonic forcing would require an unlikely coincidence of multiple weakening mechanisms, casting doubt on the feasibility of spontaneous subduction under present-day tectonic conditions (Lallemand and Arcay 2021; Arcay et al. 2020).

In this work we explore if and how an initial gravitational phase, even if it doesn't lead to a passive margin collapse resulting in a spontaneous subduction initiation, induces weakening and deformation in the margin.

In addition, we analyze how this initial phase can influence the evolution of a subsequently convergent phase in terms of SZI and eventual subduction style.

We performed 225 2D simulations using the finite-element code FALCON (Regorda et al. 2023) on a domain 3000 km wide and 700 km deep, representing a passive margin composed by a 20 Myr old oceanic lithosphere and a 90 km thick continental lithosphere.

The models undergo a first gravitational phase, simulated with free-slip lateral boundaries, that can last for 0, 10, 20 or 30 Myr. After the gravitational phase, the convergence begins, simulated by imposing a convergence velocity of 0.01, 0.05, 0.1, 0.25, 0.5 or 1 cm/yr at the lateral boundaries, along the entire lithospheric thicknesses. To investigate the response of the margin to the gravitational instability, we set up 3 viscous weakening intervals and 3 plastic laws, for a total of 9 weakening combinations.

The failure and the evolution of the passive margin have been explored in post-processing by evaluating 1) the area within a fixed distance from the trench in which the strain rate is higher than 2 10^{-14} 1/s and 2) the mean strain rate within this area.

During the gravitational phase, the models with a strong weakening combination show a strain rate localization, controlled by plastic weakening at the surface and by viscous weakening at depth, that slowly fades over time. Once the convergence begins, this damaged zone is reactivated, and for higher convergence velocity, it evolves into a subduction channel. The subduction zone initiation starts earlier in the models that experienced strain rate localization during the gravitational phase. Therefore, gravitational instabilities can trigger weakening processes capable of affecting the passive margin stability and its evolution during a convergent tectonic regime.

Acknowledgments

This research is part of Valeria Fedeli's PhD project. It has also been partially supported by the ASI - Agenzia Spaziale Italiana - project "NGGM-MAGIC - A breakthrough in understanding the dynamics of the Earth". Contract number n. 2023-22.HH.0 ASI-UNIMI

References

Arcay, Diane, Serge Lallemand, Sarah Abecassis, and Fanny Garel (2020). "Can subduction initiation at a transform fault be spontaneous?" In: Solid Earth 11. DOI: 10.5194/se-11-37-2020.

Crameri, Fabio et al. (2020). "A transdisciplinary and community-driven database to unravel subduction zone initiation". In: Nature Communications. DOI: 10.1038/s41467-020-17522-9.

Lallemand, Serge and Diane Arcay (2021). "Subduction initiation from the earliest stages to self-sustained subduction: Insights from the analysis of 70 Cenozoic sites". In: Earth-Science Reviews 221. DOI: 10.1016/j.earscirev.2021.103779.

Regorda, Alessandro, Cedric Thieulot, Iris van Zelst, Zoltán Erdős, Julia Maia, and Susanne Buiter (2023). "Rifting Venus: Insights From Numerical Modeling". In: Journal of Geophysical Research: Planets 128. DOI: 10.1029/2022JE007588.

Stern, Robert J. (2004). "Subduction initiation: Spontaneous and induced". In: Earth and Planetary Science Letters 226. DOI: 10.1016/j.epsl.2004.08.007.

Stern, Robert J. and Taras Gerya (2018). "Subduction initiation in nature and models: A review". In: Tectonophysics 746. DOI: 10.1016/j.tecto.2017.10.014.

Corresponding author: valeria.fedeli@unimi.it

XAI-Driven rainfall threshold estimation integrating GNSS data on a large landslide

R. Franceschini[1], N. Nocentini[2], A. Rosi[3], L. Tunini[1], D. Zuliani[1], G. Peressi[4], G. Rossi[1]

1 National Institute of Oceanography and Applied Geophysics – OGS, Italy
2 Department of Earth Sciences, University of Firenze
3 Department of Geosciences, University of Padova
4 Department of Civil Protection of Friuli Venezia Giulia Region

Introduction

Landslides are widespread in Italy and a major cause of casualties and infrastructure damage (Guzzetti, 2000). Slow-moving landslides can remain active for decades and respond to environmental factors such as rainfall (Hungr et al., 2014; Cascini et al., 2010; Franceschini et al., 2025). Understanding the factors controlling landslide activation is essential for hazard assessment (Borgomeo et al., 2014).
Landslide Early Warning Systems (LEWSs) often rely on rainfall thresholds, but traditional intensity–duration methods fail to account for seasonal variations or antecedent soil moisture (Glade et al., 2000; Wicki et al., 2020). Advances in GNSS technology now enable continuous, precise, and cost-effective monitoring, providing valuable data for hazard management (Benoit et al., 2015; Cina et al., 2015; Zuliani et al., 2022a).
This study (full paper available in Franceschini et al. 2025) uses a GNSS-based monitoring network to define rainfall thresholds for reactivations of the Cazzaso landslide (Udine, Italy), active since the 19th century. By combining nearly nine years of GNSS displacement data with rainfall data, an innovative machine-learning approach identifies the rainfall amount and accumulation periods most relevant to reactivation events, offering new insights into precipitation–landslide dynamics.

Study area and current monitoring system

The village of Cazzaso (Tolmezzo, Udine, NE Italy) is located at 680 m a.s.l. on an active deep-seated landslide in the Carnic Alps (Fig.1a-b). The landslide covers about 2 km², with a sliding surface reaching ~32 m depth according to inclinometer data, and an estimated mobilized volume between 10^5 and 10^7 m³ (Tunini et al. 2024), classifying it as a large landslide. The displaced material consists of glacial, fluvioglacial, lacustrine, and fluvial deposits overlying calcareous–clayey bedrock (Colucci et al. 2014), resulting in highly heterogeneous superficial layers and variable permeability that influence drainage patterns (Zuliani et al. 2022a) (Fig. 1c). Geomorphological evidence and historical documents indicate recurrent reactivations since at least 1807, including a major event in 1851 that displaced the old village by 24 m and prompted the construction of “Cazzaso Nuova” downslope. Reactivations are typically triggered by prolonged rainfall. The landslide currently moves at rates of meters per year, consistent with the “slow” category of Cruden and Varnes (1996).

Since 2016, the area has been monitored by a dedicated network operated by OGS–CRS, consisting of 12 low-cost single-frequency GPS stations installed mainly on the landslide body (Fig.1d-e), one dual-frequency geodetic GNSS station (CASO) in the village, and a seismic station coupled with a GNSS receiver (Zuliani et al. 2022b). The CASO station provides sub-millimetric precision, while all stations deliver hourly displacement data along the three spatial components, referenced to nearby stable GNSS sites of the regional FReDNet network.
Civil Protection authorities have established three daily displacement thresholds for each GNSS site (Chersich et al. 2016; Bai et al. 2020, 2022; Zuliani et al. 2022a, b):

- Yellow: >1 cm/day – increased surveillance and trend analysis;
- Orange: >2 cm/day – automatic closure of the Fusea–Cazzaso road;
- Red: >3 cm/day – evacuation of the village if exceeded by at least three stations.

Additionally, an orange-level meteorological alert for geological risk triggers the preventive closure of the Fusea–Cazzaso road.

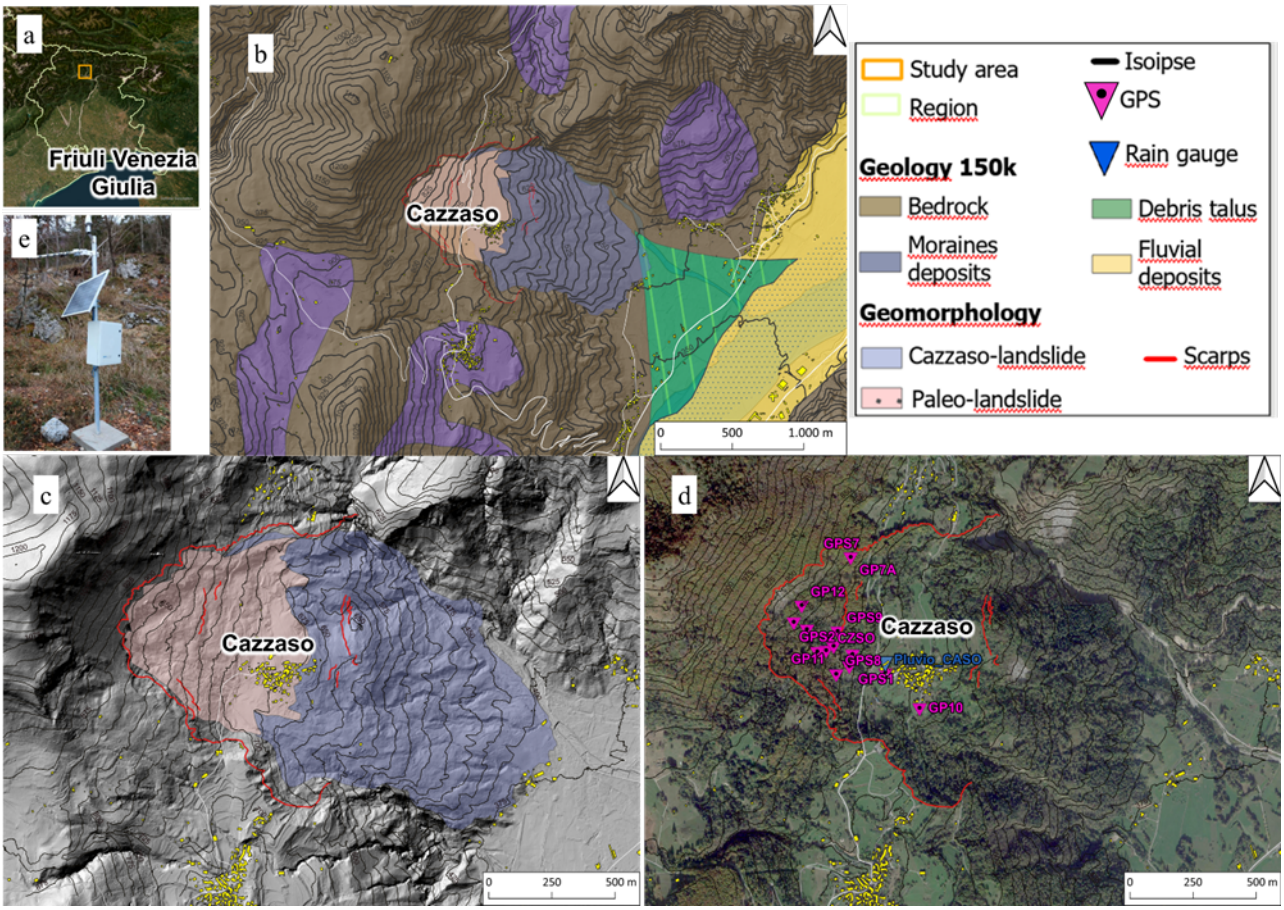

Fig. 1- In **a**) localization of the area; **b**) Geological setting of the study area; **c**) Geomorphology of Cazzaso landslide; **d**) Ortophoto and geolocalization of GNSS network. In **e**) one of the GNSS stations (in this case, GPS9).

Materials and methods

A dataset of over 540,000 GNSS observations from 12 single-frequency GPS and 2 dual-frequency GNSS stations (2015–2024) was analyzed. Displacements are computed with the double-difference

technique through the DISPLAYCE system, producing hourly–daily velocities. Hourly rainfall from two gauges (CASO on the landslide and Tolmezzo, 3.2 km away) covering 2016–2024 were processed. Erroneous or unrealistic values were removed. These datasets were used to derive rainfall thresholds.

The methodology consists of:

1. Identifying reactivations using daily GNSS velocities >1 cm/day, resulting in 116 reactivation events.

2. Computing cumulative rainfall for 1–30 days before each reactivation and discarding events unrelated to rainfall.

3. Deriving intensity–duration (I–D) thresholds using MaCumBA software.

4. Assessing antecedent rainfall importance using a Random Forest model, supported by explainable AI tools (variable importance via Out-of-Bag error and Partial Dependence Plots).

   - o Cumulative rainfall over several windows (1–10, 15, 30, 60 days) was tested.
   - o A balanced dataset (116 reactivations + 116 non-reactivations) was used.
   - o Model accuracy was evaluated using ROC–AUC.

Finally, the contribution of antecedent rainfall was compared with the performance of traditional I–D thresholds to understand whether short/intense or long-lasting rains primarily trigger the Cazzaso landslide.

Results and discussion

Analysis of GNSS and rainfall data reveals a clear seasonal pattern in landslide activity. Fig. 2a presents a comparison between rainfall record and reactivations, which occur mainly during autumn and winter (October–January), while in summer reactivations are less.

a

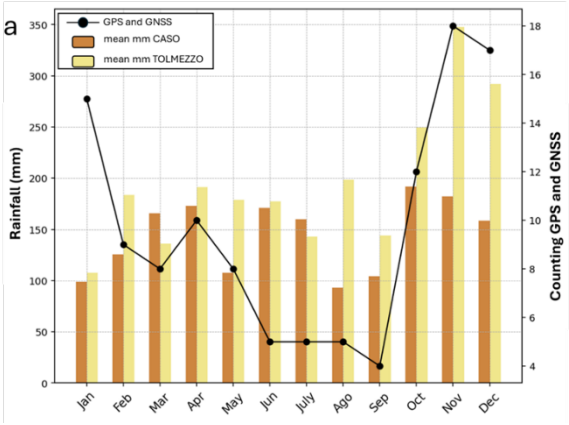

b

	CASO			Tolmezzo		
	CA	MA	FA	CA	MA	FA
Low	11	15	54	2	7	73
Moderate	7	-	8	6	-	10
High	-	-	-	-	-	-
Total	18	15	62	8	7	83
Total reactivations detected	33			15		

Fig. 2 – **a**) Comparison on monthly base between mean rainfall and number of accelerations above the velocity threshold, and **b**) I -D performance for each rain gauge. Correct Alarm (CA), MA Missed Alarm (MA) and False Alarm (FA).

Rainfall follows a similar distribution, with both CASO and Tolmezzo rain gauges recording their highest monthly totals in October and November, although the Tolmezzo station shows higher annual values due to a more complete dataset. Initial rainfall thresholds were derived using the MaCumBA I–D method. The parameters obtained for each criticality level and the corresponding performances (Fig. 2b) indicate that I–D thresholds perform poorly: they capture only a small fraction of reactivations and generate many false alarms. This suggests that the Cazzaso landslide responds to longer, multi-day rainfall periods that are not effectively represented by intensity–duration relationships, or that additional triggering factors may be involved. To better capture rainfall controls, a Random Forest (RF) model supported by XAI was applied. Model performance varied considerably between the two rain gauges: the average test AUC was 0.68 for CASO and 0.91 for Tolmezzo, highlighting the importance of continuous rainfall data. Variable importance analysis (Fig. 3) shows that medium-duration rainfall accumulations (7–9 days for CASO, 8 days for Tolmezzo) are the strongest predictors of reactivation, whereas short (1–3 days) and very long (>30 days) accumulations have limited influence. This aligns with the characteristics of the deep-seated landslide, where infiltration requires several days but is facilitated by medium-permeability glacial deposits. Partial Dependence Plots (Fig. 3) confirm this behavior: the probability of reactivation increases with cumulative rainfall, reaches a peak, and then stabilizes. Critical thresholds were identified at approximately 90 mm over 7–9 days (CASO) and 50 mm over 8 days (Tolmezzo).

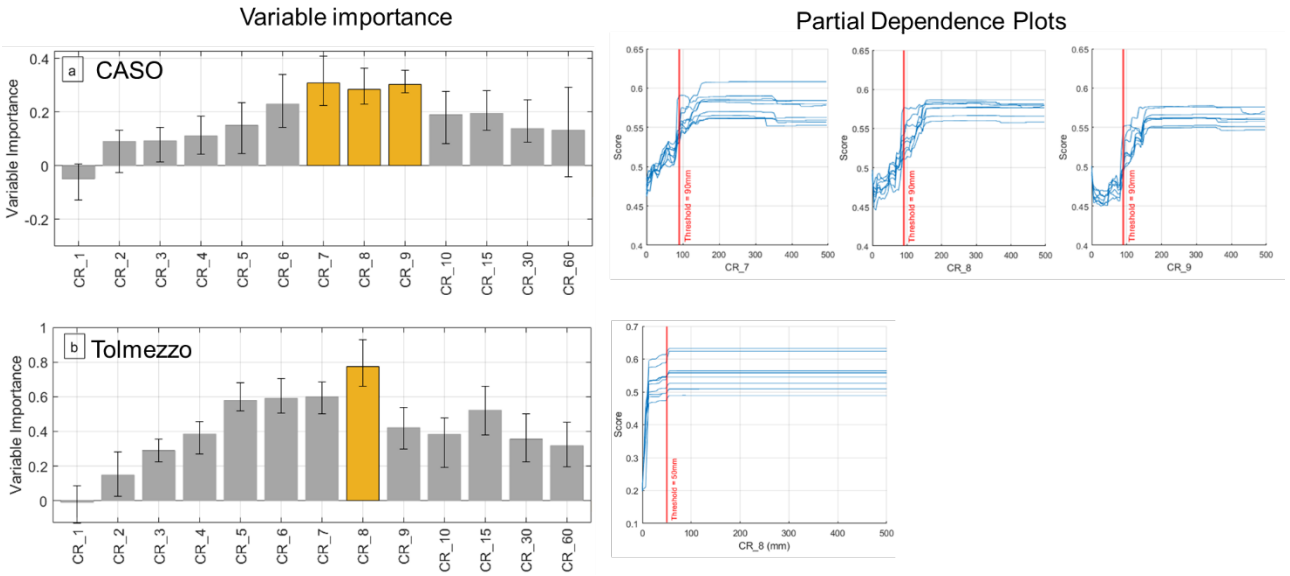

Fig. 3 - Histogram of variable importance estimates for each cumulative rainfall variable tested, along with the random variable, for the rain gauges **a**) CASO and **b**) Tolmezzo. PDPs obtained for different rainfall accumulation periods for CASO from 7 to 9 days. PDPs obtained for the 8-day cumulative rainfall by using the Tolmezzo rain gauge. Red lines indicate rainfall thresholds and correspond to peaks in the gradient of variable importance.

When comparing rainfall threshold exceedances with GNSS displacement levels (Tab. 1), no systematic correspondence emerges. Significant displacements (>3 cm/day) occur both when rainfall thresholds are exceeded and when they are not, indicating that rainfall is a key, but not exclusive, driver of accelerated movement. This highlights the need for multi-sensor, multi-parameter approaches in future LEWS implementations.

Overall, the RF–XAI framework identifies rainfall thresholds that are physically consistent with the landslide's hydrological response and outperform empirical I–D thresholds, offering a more robust basis for early warning.

	Antecedent Rainfall Threshold			
	CASO		Tolmezzo	
GNSS threshold	CR_9>90mm	CR_9<90mm	CR_8>50mm	CR_8<50mm
>1cm & <2cm	19	34	36	17
>2cm & <3cm	8	10	11	7
>3cm	20	25	25	20

Tab. 1- Performance obtained by comparing the different GNSS thresholds levels with rainfall thresholds exceedance

Conclusion

This study builds upon the monitoring system operated by CRS–OGS, which continuously collects hourly GNSS and rainfall data. By applying a displacement-based velocity threshold, a catalogue of landslide reactivations was created and used to explore rainfall controls. Traditional I–D thresholds proved ineffective, as the Cazzaso landslide is not triggered by short, high-intensity events. Therefore, a machine-learning approach with interpretable tools was adopted. Partial Dependence Plots enabled a clear assessment of how different rainfall accumulation periods influence reactivation, revealing that 8-day cumulative rainfall is the most significant predictor. This provides a reliable rainfall threshold that can complement GNSS monitoring for operational warning purposes. Although developed for this specific case, the method is broadly applicable to other landslide settings. Thresholds should, however, be periodically updated as new GNSS data become available and as rainfall patterns evolve under climate change.

Acknowledgements

This study was carried out within the RETURN Extended Partnership and received funding from the European Union Next-GenerationEU (National Recovery and Resilience Plan – NRRP, Mission 4, Component 2, Investment 1.3 – D.D. 1243 2/8/2022, PE0000005)

The authors wish to thank the Civil Protection of the Friuli Venezia Giulia Region, for the collaboration in the realization of the early warning system described in this paper and for the precious work in collaboration with Center for Seismological Research (CRS - National Institute of Oceanography and Applied Geophysics – OGS) for the monitoring system.

References

Bai D, Tang J, Lu G, Zhu Z, Liu T, & Fang J (2020). The design and application of landslide monitoring and early warning system based on microservice architecture. Geomatics, natural hazards and risk, 11(1), 928-948. https://doi.org/10.1080/19475705.2020.1766580

Benoit L, Briole P, Martin O, Thom C, Malet JP, & Ulrich P (2015). Monitoring landslide displacements with the Geocube wireless network of low-cost GPS. Engineering geology, 195, 111-121. https://doi.org/10.1016/j.enggeo.2015.05.020

Borgomeo E, Hebditch KV, Whittaker AC, & Lonergan L (2014). Characterising the spatial distribution, frequency and geomorphic controls on landslide occurrence, Molise, Italy. Geomorphology, 226, 148-161.

Cascini L, Cuomo S, Pastor M, & Sorbino G (2010). Modeling of rainfall-induced shallow landslides of the flow-type. Journal of geotechnical and geoenvironmental engineering, 136(1), 85-98.

Chersich M, Curone D, Devoti R, Galvani A, Osmo M, & Sepe V (2016). Benchmark Test of a GNSS Low-Cost, Single-Frequency, Geodetic Monitoring System; Società Geologica Italiana: Naples, Italy, 2016. https://doi.org/10.3390/s22093526

Cina A, & Piras M (2015). Performance of low-cost GNSS receiver for landslides monitoring: Test and results. Geomatics, Natural Hazards and Risk, 6(5-7), 497-514. https://doi.org/10.1080/19475705.2014.889046

Colucci RR, Monegato G, & Žebre M (2014). Glacial and proglacial deposits of the Resia Valley (NE Italy): new insights on the onset and decay of the last Alpine Glacial Maximum in the Julian Alps. Alpine and Mediterranean Quaternary, 27(2), 85-104. https://amq.aiqua.it/index.php/amq/article/view/75.

Cruden DM, & Varnes DJ (1996). Landslide types and processes. In: Turner AK, Schuster RL (eds) Landslides investigation and mitigation. Transportation research board, US National Research Council. Special Report 247, Washington, DC, Chapter 3, pp. 36–75

Franceschini, R., Nocentini, N., Rosi, A., Tunini, L., Zuliani, D., Peressi, G., & Rossi, G. (2025). Deriving rainfall thresholds with XAI and GNSS measurements for a large landslide. Landslides, 1-14.

Glade T, Crozier M, & Smith P (2000). Applying probability determination to refine landslide-triggering rainfall thresholds using an empirical “Antecedent Daily Rainfall Model”. Pure Appl Geophys 157:1059–1079. https://doi.org/10.1007/s000240050017

Guzzetti F (2000). Landslide fatalities and evaluation of landslide risk inItaly. Eng Geol 58:89–107. https://doi.org/10.1016/S0013-7952(00)00047-8

Hungr O, Leroueil S, & Picarelli L (2014). The Varnes classification of landslide types, an update. Landslides, 11, 167-194. https://doi.org/10.1007/s10346-013-0436-y

Tunini L, Zuliani D, Di Traglia F, Borselli L, De Luca C, Nolesini T, & Casu F (2024). Monitoring and modelling moraine landslides: an example from Cazzaso village (Carnic Alps, Italy). Bulletin of Geophysics and Oceanography, Vol. 65, n. 3, 327-346. doi: 10.4430/bgo00459

Wicki A, Lehmann P, Hauck C, Seneviratne SI, Waldner P & Stähli M (2020). Assessing the potential of soil moisture measurements for regional landslide early warning. Landslides, 17, 1881-1896. https://doi.org/10.1007/s10346-020-01400-y

Zuliani D, Tunini L, Di Traglia F, Chersich M, & Curone D (2022a). Cost-effective, single-frequency GPS network as a tool for landslide monitoring. Sensors, 22(9), 3526. https://doi.org/10.3390/s22093526

Zuliani D, Tunini L, Severin M, Bertoni M, Ponton C, & Parolai S (2022b). LZER0: A Cost-Effective Multi-Purpose GNSS Platform. Sensors, 22(21), 8314. https://doi.org/10.3390/s22218314

Corresponding author: Rachele Franceschini; *Email: rfranceschini@ogs.it

GEODETIC LINKING ADVANCED SOFTWARE SYSTEM (GLASS) AND THE CENTRAL AND EAST EUROPEAN GNSS NODE FOR EPOS (CEGNxEPOS)

S. Galvi[1], E. Magrin[1], L. Tunini[1], A. Magrin[1], P. Fabris[1], G. Rossi[1], A. Compagno[1], M. Bertoni[1], E. Del Negro[1], D. Zuliani[1], M. Furlan[2], B. Stopar[3], O. Sterle[3], K. Ritlop[3]

[1] Istituto Nazionale di Oceanografia e di Geofisica Sperimentale – OGS, Italy
[2] Insiel S.p.A., Divisione Pubblica Amministrazione Digitale, Servizi e sistemi per ambiente, territorio e agricoltura, Italy
[3] University of Ljubljana, Faculty of Civil and Geodetic Engineering, Slovenia

Introduction

The European Plate Observing System (EPOS https://www.epos-eu.org/) integrates geophysical and geodetic data to support Solid Earth research, providing harmonised access to observations and derived products. Within this framework, OGS has developed and now operates the Central and East European GNSS Node for EPOS (CEGNxEPOS), a cross-border data node that aggregates GNSS data from northeastern Italy and neighbouring countries. The node relies on the Geodetic Linking Advanced Software System (GLASS, Fernandes et al. 2022), designed for federated GNSS data distribution and interoperability with the EPOS GNSS Data and Products Thematic Core Service (TCS).

The GLASS Node at OGS

In the context of the EPOS-Italy Joint Research Unit (JRU) (https://www.epos-italia.it/it), OGS has installed and configured a complete GLASS node for automated ingestion, harmonisation, validation and distribution of GNSS data. OGS manages the node as CEGNxEPOS (see Fig. 1), integrating observations from the following infrastructure:

- **FReDNet** geodetic network (Zuliani et al. 2018, https://frednet.crs.ogs.it/en/)
- **Antonio Marussi** GNSS network of the Autonomous Region of Friuli Venezia Giulia (https://rem.regione.fvg.it/)
- GNSS permanent sites and networks from Slovenia and Austria in collaboration with:
    - **University of Ljubljana**, Faculty of Civil and Geodetic Engineering (Tunini et al. 2024);
    - the non-profit organisation Zavod **MPRI**, raziskovalna in razvojna dejavnost (Tunini et al. 2024);
    - Wiener Netze **GmbH** for some GNSS sites belonging to the **EPOSA** network (https://www.eposa.at/englisch).

  OGS also collaborates, on GNSS-related activities, with the **Veneto Region** (https://www.regione.veneto.it/web/ambiente-e-territorio/stazioni-gps) and with the University of Padua (https://www.unipd.it/en/), their stations are currently undergoing hardware upgrades and are therefore not yet included in the node.

OGS has also initiated a collaboration agreement with the Austrian Federal Office of Metrology and Surveying (**BEV**), which will enable the distribution through the OGS GLASS node of six additional stations of the Austrian Positioning Service (**APOS** https://www.bev.gv.at/en/Services/Products/Austrian-POsitioning-Service.html)

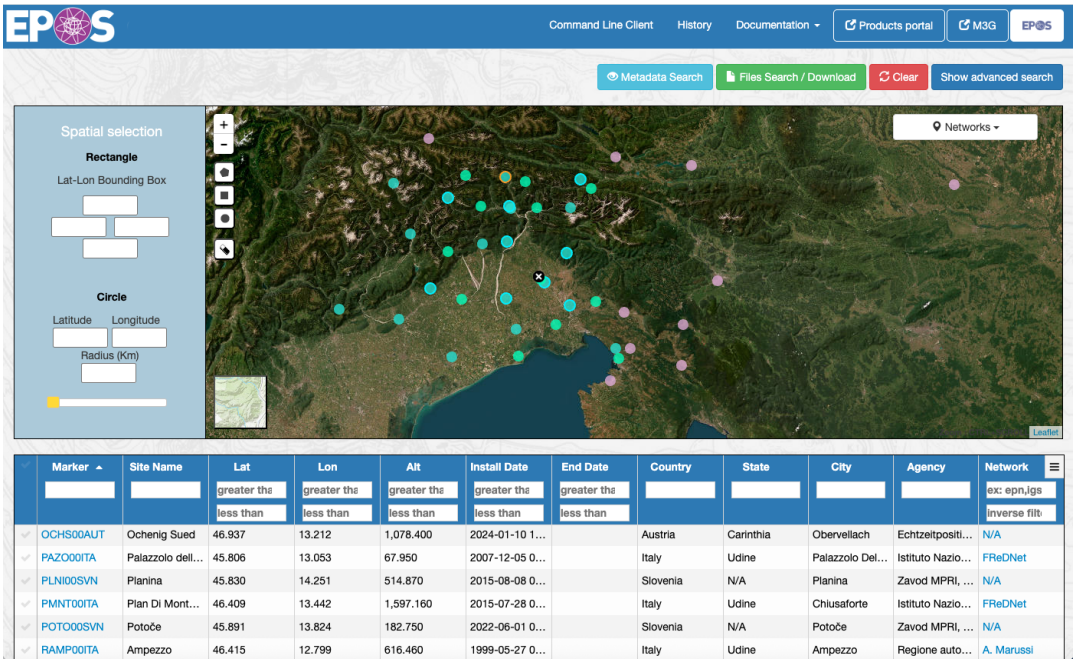

Fig. 1: The CEGNxEPOS GLASS node managed by OGS, with GNSS sites located in northeastern Italy and in the surrounding cross-border regions.

The node provides standardised and **F**indable, **A**ccessible, **I**nteroperable and **R**eusable (FAIR) GNSS data to EPOS, supporting crustal deformation studies across a region of significant tectonic interest. The GLASS services expose EPOS-ready metadata, RINEX files, quality indicators and discovery functionalities through a federated architecture.

Public access:

- http://gnssdata-epos.ogs.it
- https://frednet.crs.ogs.it/en/gnss-data-gateway/

Recent Developments: 2025 Completion of the Fully (O)perational Stage

During previous years, OGS progressively advanced through all official EPOS GNSS Data Gateway stages: Planned, Under testing, Pre-operational, and Operational (partly populated), as part of Objective 1 of the EPOS-Italy programme. In 2025, OGS successfully completed this objective, achieving the **Fully (O)perational status** (see https://gnss-metadata.eu/MOID/datadistributor.64dca7bf92026d043605e332)

This required full population of the dataset exposed via GLASS, harmonisation of metadata and RINEX formats, integration of networks in Italy, Slovenia and Austria, and validation activities with

the Data Gateway Working Group (DWG). The transition certifies the maturity and stability of the CEGNxEPOS node within EPOS.

OGS Accession to the EPOS-GNSS Consortium Board

Following the operational consolidation of the node, OGS formally acceded to the EPOS-GNSS Consortium Agreement in 2025, becoming a full Party of the Thematic Core Service GNSS. Through the accession form, OGS appointed its representative to the Consortium Board, the TCS's main strategic and decision-making body of the TCS. This recognises OGS as both a data provider and an institutional actor in the governance and development of the EPOS GNSS infrastructure.

Scientific and Operational Impact

The GLASS-based CEGNxEPOS node provides harmonised and validated GNSS data for crustal deformation studies (Tunini et al. 2024), enhances cross-border interoperability, and contributes directly to EPOS GNSS services. It improves observational coverage in a key tectonic region and promotes long-term, coordinated GNSS data management practices.

Conclusions

The achievement of the Fully (O)perational status and the formal entry of OGS into the EPOS-GNSS Consortium Board represent major milestones for the Italian geodetic community. They confirm the strategic importance and maturity of the CEGNxEPOS node and establish OGS as a key contributor to EPOS governance and future GNSS developments.

Acknowledgments

Activities were carried out within the EPOS-Italy JRU framework, in collaboration with the EPOS GNSS Data Gateway Working Group, the colleagues from the Istituto Nazionale di Geofisica e Vulcanologia (INGV) involved in the EPOS-GNSS activities, the national and international GNSS network operators, and regional and institutional partners supporting GNSS monitoring activities, including the Regione Autonoma Friuli Venezia Giulia for providing access to data from the Antonio Marussi GNSS network, and INSIEL S.p.A., the in-house ICT company of the Friuli Venezia Giulia Region, which provides digital services and operational support to regional and local public administrations. INSIEL manages the Marussi Network on behalf of the Regione Autonoma Friuli Venezia Giulia, ensuring its full usability, the colleagues from the non-profit organisation Zavod MPRI, the EPOSA team and University of Ljubljana Faculty of Civil and Geodetic Engineering members. This work has been financially supported by the EPOS Research Infrastructure through the contribution of the Italian Ministry of University and Research (MUR) - EPOS ITALIA Joint Research Unit, through RI-SI-EPOS contribution of Republic of Slovenia, Ministry of Education, Science and Sport, the European Union from the European Regional Development Fund and through support from the Slovenian Research Agency through research core fundings No. P2-0227 and No. P1-0419 and NRRI/ESFRI project EPOS No. I0-E017.

References

- Fernandes, R.; Bruyninx, C.; Crocker, P.; Menut, J.-L.; Socquet, A.; Vergnolle, M. .; Avallone, A.; Bos, M.; Bruni, S.; Cardoso, R.; Carvalho, L.; Cotte, N.; D'Agostino, N. .; Deprez, A.; Andras, F. .; Geraldes, F.; Janex, G.; Kenyeres, A.; Legrand, J.; Ngo, K.-M.; Lidberg, M.; Liwosz, T.; Manteigueiro, J.; Miglio, A. .; Soehne, W.; Steffen, H.; Toth, S.; Dousa, J.; Ganas, A.; Kapetanidis, V.; Batti, G. A New European Service to Share GNSS Data and Products. *Ann. Geophys.* **2022**, *65* (3), DM317. https://doi.org/10.4401/ag-8776;
- Tunini L.; Magrin A.; Rossi G.; Zuliani D. Global Navigation Satellite System (GNSS) time series and velocities about a slowly convergent margin processed on high-performance computing (HPC) clusters: products and robustness evaluation. (**2024**) Earth System Science Data, 16 (2), pp. 1083 – 1106, https://essd.copernicus.org/articles/16/1083/2024;

- Zuliani D., Fabris P., Rossi G. (2018). FReDNet: Evolution of a Permanent GNSS Receiver System. In: Cefalo R., Zieliński J., Barbarella M. (eds) *New Advanced GNSS and 3D Spatial Techniques. Lecture Notes in Geoinformation and Cartography*. Springer, Cham, First Online: doi:10.1007/978-3-319-56218-6_10;

Understanding Magma Ascent through Heat Propagation Buoyancy and Thermal Loss in the Lithosphere

C. Godano[1], M. Gorgone[2], C. F. Munafò[2], S. Carlino[3], P. Rogolino[2] and F. Oliveri[2]

[1]Department of Mathematics and Physics, University of Caserta "Luigi Vanvitelli" viale Lincoln, 5, 81100 Caserta, Italy
[2]Department of Mathematical and Computer Sciences, Physical Sciences and Earth Sciences, University of Messina, viale F. Stagno d'Alcontres, 31, 98166 Messina, Italy
[3]Istituto Nazionale di Geofisica e Vulcanologia - Sezione di Napoli - Osservatorio Vesuviano, Napoli, Italy

We introduce a rather simple model for the ascent of the magma through the lithosphere, based on a mix of conduction, rock partial melting, and buoyancy, where we take into account the heat dissipation due to the melting process. Under suitable assumptions, a hyperbolic linear partial differential equation describing the process is derived from a general thermodynamical model whose constitutive equations are compatible with the second principle of thermodynamics. Then, we derive numerically a solution to a physically meaningful initial/boundary condition that can explain many of the experimental observations. More precisely, we suggest a mechanism for the magma emplacement able to explain the different depths of emplacement depending on one of the model parameters. Moreover, this parameter can be tuned to obtain the disappearance of the emplacement, which justifies the occurrence of hot spots.

Strain Deformation-Driven Cascades Explains Volcanic Earthquake Swarms

Cataldo Godano[1], Vincenzo Convertito[2], Anna Tramelli[2], Umberto Tammaro[2], Valentina Bruno[3], Giuseppe Petrillo[4]

[1]Department of Mathematics and Physics, Università' della Campania
[2]INGV, Osservatorio Vesuvianio
[3]INGV, Osservatorio Etneo
[4]Earth Observatory of Singapore, Nanyang Technological University

Volcanic earthquake swarms are among the most enigmatic precursors of eruptions, often reflecting the interplay between deformation, fluid migration, and fault activation. Yet, a unifying quantitative law linking deformation to swarm productivity has remained elusive.
Here we show that, across six active volcanic systems worldwide, the cumulative number of earthquakes grows as a double-exponential function of ground deformation, revealing a universal deformation-driven scaling. This relationship naturally emerges from an epidemic-type model in which the triggering efficiency is modulated by deformation and limited by saturation effects. The model reproduces the observed behaviour across volcanic environments ranging from fluid-driven calderas to rift-related volcanoes.
The fitted parameters constrain the relative roles of elastic loading and plastic dissipation, suggesting that swarm evolution results from the competition between strain accumulation and relaxation in a disordered, velocity-strengthening medium. These findings identify a universal physical mechanism underlying swarm generation and provide a predictive framework for linking ground deformation to seismic hazard at active volcanoes.

The new Center for National Gravimetric Service

Filippo Greco[1], Giovanna Berrino[1], Federica Riguzzi[1], Daniele Sampietro[1,2], Mattia Crespi[1,3,4,5], Fernando Sansò[1,2,5]

[1] *Istituto Nazionale di Geofisica e Vulcanologia (INGV)*
[2] *GReD s.r.l., via Valleggio 11, Como, Italy*
[3] *Geodesy and Geomatics Division-DICEA, Sapienza University of Rome, via Eudossiana 18, Rome, Italy*
[4] *Sapienza School for Advanced Studies, Sapienza University of Rome, viale Regina Elena 295, Rome, Italy*
[5] *Accademia Nazionale dei Lincei*

The Center for National Gravimetric Service (hereinafter referred to as CSGN), has been recently established as an interdepartmental structure of the Istituto Nazionale di Geofisica e Vulcanologia (INGV) with the aim of coordinating, managing, developing, and enhancing activities related to the measurement of the Earth's gravitational field in Italy. These activities are carried out within the framework of the National Reference Gravimetric Network, the Italian Fiducial Gravimetric Network, and aerogravimetric surveys conducted throughout Italy. The CSGN will have also the aim to disseminate gravity field data, such as gravitational anomalies and geoid undulations, to the national and international scientific community, as well as to the public.

The establishment of the CSGN is grounded in a set of scientific, technical, and organizational considerations that justify its creation and define its strategic role within INGV. In particular:

1.0 Implementation of a national gravity–geoid database

A coherent, consistent, and regularly updated national database of gravity and geoid data is planned for the near future. This database will cover the entire country, including data from aerogravimetric surveys, funded by the Ministry of the Environment and Energy Security (MASE). It is the task of the Center to provide on request the best prediction of point gravity anomalies and geoid values, using all existing data including the new digital model of the terrain for the purpose of computing the most accurate terrain corrections.

2.0 Italian Fiducial Gravimetric Network

INGV is engaged in the development of the Italian Fiducial Gravimetric Network, which will consist of approximately ten stations evenly distributed across the national territory (Fig. 1). They are planned to be realized with superconducting and absolute gravimeters in continuous (or quasi-continuous) recording. Some of these stations are already operational in Nicolosi (INGV facility), Cascina (Virgo facilities) and Napoli (CESMA – University of Napoli “Federico II”), while others will be installed in the near future. The primary objective of this network is to monitor long-term, -wavelength temporal variations in the gravity field, particularly in seismic and volcanic areas.

3.0 G0 and H0 reference networks

Based on two projects (Pianeta Dinamico, funded by INGV and PRIN2020, funded by MUR), and in collaboration with Politecnico di Milano, INRIM, Sapienza University of Rome, and ASI, INGV is developing the national G0 gravimetric and H0 height reference networks, based on high-precision

absolute gravity and height measurements (Fig. 2). This infrastructure constitutes a modern gravimetric and height reference frame for Italy, aligned with European and international standards, and it is intended to support a wide range of scientific and technological activities in geodesy and geophysics (Greco et al., 2024; Barzaghi et al., 2026). This reference frame, which could be integrated with new stations in the future, will be useful to: a) homogenize all the gravimetric and height data of different origins already available across the Italian territory, leading to the revision of the current national gravimetric/height database; b) homogenize Bouguer anomaly maps at all scales; c) reference all the new gravimetric surveys conducted on the national territory, at different scales and for different purposes, to a single system; d) reprocess all the available gravimetric data in order to refine the Moho.

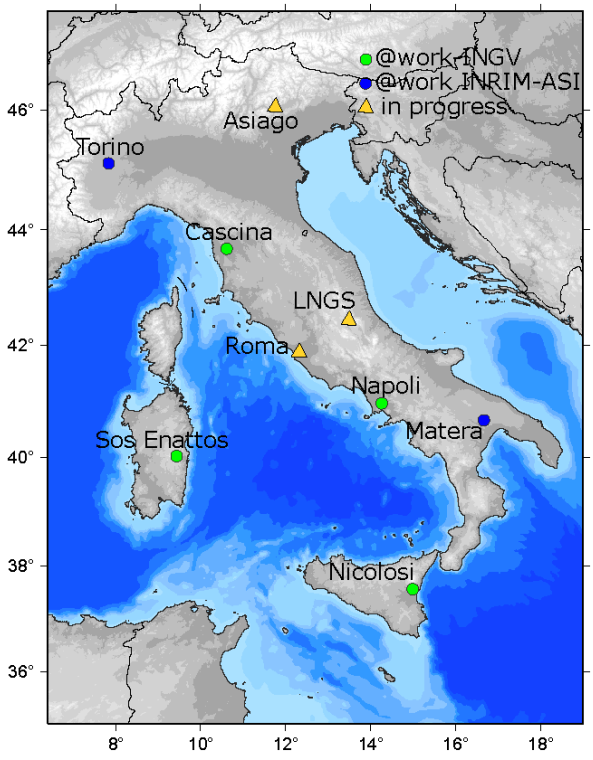

Fig.1 The Italian Fiducial Gravimetric Network for continuous measurements.

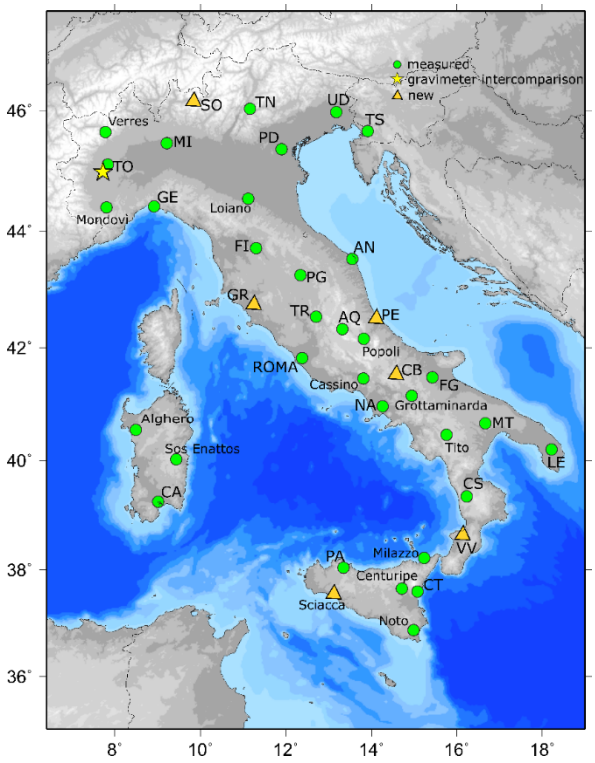

Fig. 2 – The new absolute gravity G0 and height H0 reference networks: measured stations (green dots); Italian site of gravimeter intercomparison (INRIM; yellow star); stations still to be measured (yellow triangles).

Acknowledgments

We thank the INGV President, Fabio Florindo, and the INGV leadership for believing in and approving the establishment of the CSGN.

References

Barzaghi et al.; 2026: The new reference gravity network in Italy. Bulletin of Geophysics and Oceanography, in publication

Greco F., Berrino G., Riguzzi F. et al.; 2024: The first absolute gravity and height reference network in Sicily. Scientific Data, 11, 357, DOI 10.1038/s41597-024-03177-4

Corresponding author: filippo.greco@ingv.it

Numerical analyses of 3D seismic site response in the Norcia sedimentary basin (Central Italy)

F. Linsalata[1], R. Puglia[2], A. Costanzo[3], M. Massa[2], S. Lovati[2], C. Smerzini[4], M. Pischiutta[1], M. Vanini[4], S. Parolai[5], A. d'Onofrio[6] and F. Silvestri[6]

[1] Istituto Nazionale di Geofisica e Vulcanologia, Rome, Italy
[2] Istituto Nazionale di Geofisica e Vulcanologia, Milan, Italy
[3] Istituto Nazionale di Geofisica e Vulcanologia, Osservatorio Nazionale Terremoti, Rome, Italy
[4] Department of Civil and Environmental Engineering, Politecnico di Milano, Milan, Italy
[5] Department of Mathematics, Informatics and Geosciences, University of Trieste, Italy
[6] Department of Civil, Architectural and Environmental Engineering, University of Napoli, Naples, Italy

The Norcia basin, located in the central Apennines, is a Quaternary intermontane depression strongly affected by major seismic events, including the Mw 6.5 earthquake of 30 October 2016. Its complex geological setting, characterized by lacustrine, palustrine, alluvial and conglomeratic deposits overlying a carbonate bedrock, makes it an ideal natural laboratory for investigating 3D seismic site amplification effects. Within the INGV PD-GEMME project, we developed an integrated geological and geophysical model of the basin, combining new field data including MASW profiles, passive seismic arrays, and stratigraphic boreholes with information from the scientific literature (*e.g.* Bindi *et al.* 2011*;* Di Giulio *et al.* 2020) and microzonation studies (https://sisma2016data.it/microzonazione/). The 3D numerical model has been implemented using the computational codes SPEED and FLAC3D.
Although both codes can perform non-linear simulations, model validation is carried out in the linear domain using weak-motion recordings from the temporary seismic network 3H-2009, which captured several events of the 2009 L'Aquila sequence. The results highlight the significant role of basin geometry, sediment heterogeneity, and bedrock velocity structure in shaping the amplification patterns, especially within the 0.5-8 Hz frequency range. This is particularly relevant for understanding the amplifications that affected the basin during the seismic sequence. Ongoing work focuses on improving the goodness-of-fit between simulations and observations and extending the modelling to non-linear conditions, aiming to reproduce the site effects induced by the strong-motion during the 2016 Central Italy sequence. .

keyword: 3D numerical simulations, local seismic response, earthquakes

References

Bindi D. et al. (2011) - Site effects observed in alluvial basins: the case of Norcia (Central Italy). Bulletin of Earthquake Engineering, *9*, 1941-1959, https://doi.org/10.1007/s10518-011-9273-3

Di Giulio G. et al. (2020) - Investigation of the Norcia basin (Central Italy) through ambient vibration measurements and geological surveys. Engineering Geology *267*, 105501, https://doi.org/10.1016/j.enggeo.2020.105501

CentroMS, https://www. centromicrozonazionesismica.it/en/

Laboratory Seismic Characterization of the Adriatic Plate Lithospheric Mantle and Continental Crust

Lopez M.C.*[1], Kastelic V.[2], Carafa M. M. C[2], Gola G [3] ,Vinciguerra S[4], Motra H[5], Zanetti A[1,3]

[1] Department of Earth and Environmental Sciences (DSTA), University of Pavia
[2] Istituto Nazionale di Geofisica e Vulcanologia – INGV, Roma1, L'Aquila
[3] Institute of Geosciences and Earth Resources (IGG), Italian National Research Council (CNR)
[4] Department of Earth Sciences, Università degli Studi di Torino
[5]Department of geosciences, University of Kiel

Seismological models of the continental crust are commonly limited by the scarcity of petrophysical constraints and the non-uniqueness of seismic velocity–lithology relationships, as different rock types may exhibit similar velocities. To address this limitation, within the framework of the PEACE Project, we assembled a comprehensive petrophysical, thermal and geochemical dataset of over 100 rock samples from the Adriatic plate, representing an idealized vertical lithospheric profile. Among these, 45 samples were collected from the Ivrea–Verbano Zone (IVZ) in the western Southern Alps to specifically characterize the lithospheric mantle and the lower and upper continental crust.

The dataset includes ultramafic mantle rocks (peridotites and pyroxenites), lower-crustal lithologies (mafic and felsic granulites, amphibolites), and upper-crustal rocks (metagabbros, granites, calc-silicates, mylonites).

All samples underwent extensive petrophysical characterization at ambient laboratory conditions. Compressional- and shear-wave velocities (Vp and Vs) were measured under dry (unsaturated) conditions, alongside density, porosity, thermal conductivity, and seismic anisotropy. Petrographic observations and quantitative mineral chemistry obtained by electron microprobe analyses were used to assess the influence of mineral composition, modal abundance, alteration, texture, and grain size. Existing literature data were critically reviewed, and mineralogical compositions were verified to ensure consistency and reliability, enabling the classification of samples into well-defined lithological categories. To approximate in-situ lithospheric conditions, selected lower-crustal and upper-mantle lithologies were further investigated under high-pressure and high-temperature conditions (12–600 MPa; 20–600 °C) using ultrasonic measurements in a Multi-Anvil Apparatus.

Laboratory results reveal clear mineralogical and textural controls on seismic properties. Peridotites exhibit the highest Vp (6.99–7.81 km/s) and densities (3.25–3.38 g/cm³), primarily controlled by olivine content. Pyroxenites show slightly lower Vp (6.31–7.49 km/s) and densities (2.99–3.38 g/cm³), reflecting both the abundance and type of pyroxene present, with clinopyroxene producing

higher velocities than orthopyroxene, as well as plagioclase content. Garnet-bearing mafic granulites have higher Vp (6.0–6.3 km/s) and densities (2.9–3.1 g/cm³) than garnet-free equivalents. Felsic granulites display largely variable Vp (5.9–6.5 km/s) and densities (2.57–2.92 g/cm³), controlled primarily by the relative abundance of quartz and garnet. Amphibolites also exhibit a wide range of Vp (5.52–7.34 km/s) and densities, reflecting differences in their protoliths and metamorphic processes with hornblende- and plagioclase-rich samples having higher velocities than carbonate-bearing ones.

Metagabbros show Vp and density ranges overlapping those of the mafic granulites, as they are controlled by similar mineral phases (garnet, amphibole, plagioclase). Granitic rocks are characterized by low densities (2.57–2.61 g/cm³) and moderate Vp (5.94–6.49 km/s) which are mostly controlled by the feldspar and quartz content, whereas calc-silicates and mylonites display reduced velocities related to carbonate and mica content, with mylonites additionally exhibiting strong seismic anisotropy from foliation.

The results highlight the strong influence of mineral assemblage, microstructure, and fluid content on Vp–Vs relationships and demonstrate how laboratory-derived velocities can be used to calibrate and refine geophysical models based on geophysical observations. Together, these integrated petrophysical and petrographic datasets provide new constraints on the thermo-rheological structure of the Adriatic plate and contribute to improved interpretation of seismic tomography and lithospheric-scale geophysical models.

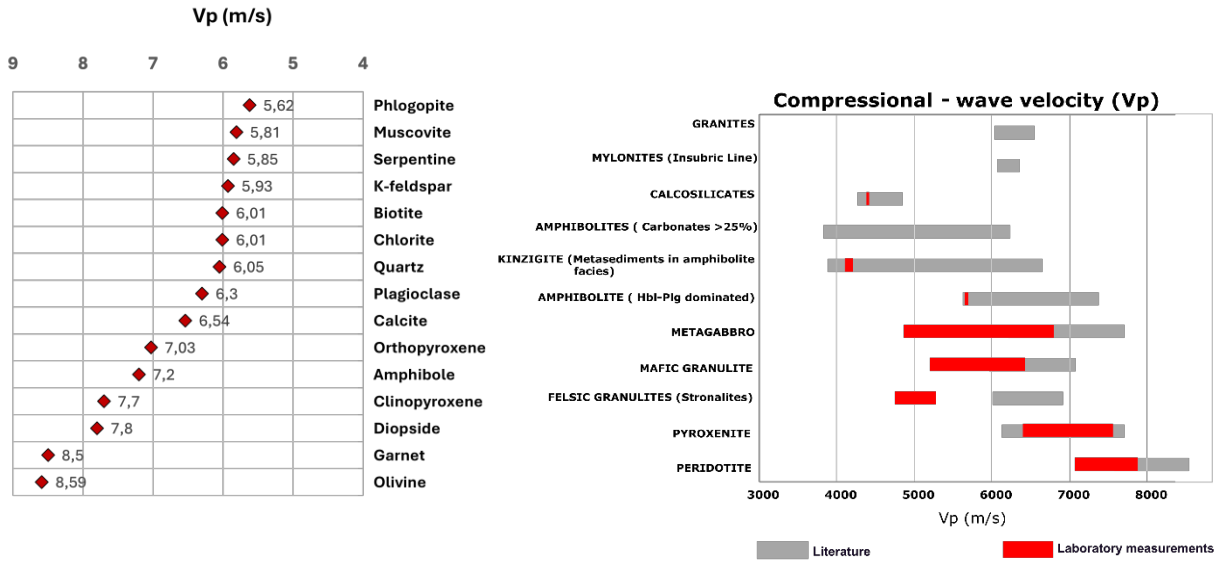

Fig. 1. (a) Compressional (P-wave) velocities of selected rock-forming minerals and rocks compiled from the literature (Kern et al., 2009). (b) Compressional-wave velocities Vp measured under dry, ambient laboratory conditions for upper-crustal, lower-crustal, and lithospheric mantle rocks. Gray bars represent literature values, whereas red bars show laboratory measurements.

References

Barruol, G., & Mainprice, D. (1993). 3-D seismic velocities calculated from lattice-preferred orientation and reflectivity of a lower crustal section: examples of the Val Sesia section (Ivrea zone, northern Italy). *Geophysical Journal International*, *115*(3), 1169-1188.

Burke, M. M., & Fountain, D. M. (1990). Seismic properties of rocks from an exposure of extended continental crust—new laboratory measurements from the Ivrea Zone. *Tectonophysics*, *182*(1-2), 119-146.

Di Stefano, R., & Ciaccio, M. G. (2014). The lithosphere and asthenosphere system in Italy as inferred from the Vp and Vs 3D velocity model and Moho map. *Journal of Geodynamics*, *82*, 16-25.

Kern, H., Mengel, K., Strauss, K. W., Ivankina, T. I., Nikitin, A. N., & Kukkonen, I. T. (2009). Elastic wave velocities, chemistry and modal mineralogy of crustal rocks sampled by the Outokumpu scientific drill hole: Evidence from lab measurements and modeling. *Physics of the Earth and Planetary Interiors*, *175*(3-4), 151-166

Khazanehdari, J., Rutter, E. H., & Brodie, K. H. (2000). High-pressure-high-temperature seismic velocity structure of the midcrustal and lower crustal rocks of the Ivrea-Verbano zone and Serie dei Laghi, NW Italy. *Journal of Geophysical Research: Solid Earth*, *105*(B6), 13843-13858.

Corresponding author:mariacamila.lopezsuarez01@universitadipavia.it

Empirical fitting of the Brune source model from high-rate GPS solutions for rapid magnitude estimation

P. Miele[1], A. Avallone[1], A. Herrero[2], F. Bernardi[2], S. Lorito[2], A. Piatanesi[2], F. Romano[2]

[1] Istituto Nazionale di Geofisica e Vulcanologia, Sezione Irpinia, Grottaminarda, Italy
[2] Istituto Nazionale di Geofisica e Vulcanologia, Sezione ONT, Rome, Italy

Current Earthquake and Tsunami Early Warning Systems (ETEWSs) worldwide utilize ground motion observations from strong-motion accelerometers and broadband seismometers for the rapid estimation of magnitude, hypocenter, and other source parameters to characterize the distribution and intensity of strong shaking. While traditional inertial sensors perform well for magnitude estimation of small-to-moderate-size events *(Allen and Melgar, 2019)*, generally they struggle to record the full dynamic range of ground displacements, especially at low frequencies, that is below the relative corner frequency. This limitation is particularly acute during large earthquakes (Mw>7) that are dominated by near-field body forces generated from the source *(Melgar et al., 2013; Crowell, 2024)*. This represents a significant challenge for early warning algorithms attempting to estimate source parameters in real time, especially for these extremely damaging, large-magnitude events that are potentially tsunamigenic as well.

To overcome this limitation, geodetic data, specifically GNSS displacements, have been proposed for or incorporated into earthquake and tsunami early warning algorithms *(Sobolev et al., 2007; Crowell et al., 2009, 2016;Hoechner et al, 2012; Grapenthin et al., 2014; Minson et al., 2014; Murray et al., 2018, 2023)* and ground-motion models (GMMs; *Goldberg et al., 2021; Crowell et al., 2023)* as a crucial complement to traditional seismic approaches. This study focuses on leveraging real-time high-rate Global Navigation Satellite System (GNSS) observations (>1Hz), which provide high-fidelity ground displacement recordings essential for swift magnitude estimation.

We have considered a database of moderate magnitude (Mw 5 – 6.5) seismic events in the Mediterranean region for which high-rate GNSS solutions were obtained. For each event with a known moment magnitude, an empirical scaling factor was derived to fit the observed displacement spectrum to the theoretical Brune source model low-frequency plateau *(Brune, 1970)*. The primary objective of this research is to analyze the stability and potential variations of this derived scaling factor across the compiled event catalogue. Verifying the existence of a robust or "general" scaling factor is crucial, as it could be directly applied for the rapid estimation of

magnitude in the immediate aftermath of future moderate-to-large seismic events, significantly enhancing ETEWS performance.

The work presents the first results with the proposed approach and discusses in particular the major observed features (or lack thereof) in the scaling factor. Particular attention is given to the criticalities encountered and the relationship between the derived scaling factors and the specific source characteristics of the events, including their radiation pattern and focal mechanism.

References

Allen, R. M., and D. Melgar (2019). Earthquake early warning: Advances, scientific challenges, and societal needs, Annu. Rev. Earth. Planet. Sci. 47, 361–388, doi: 10.1146/annurev-earth-053018-060457.

Brune, J. N. (1970). Tectonic stress and the spectra of seismic shear waves from earthquakes, J. Geophys. Res. 100, no. 26, 4997–5009.

Crowell, B. W., Y. Bock, and M. B. Squibb (2009) Demonstration of earthquake early warning using total displacement waveforms from real-time GPS networks, Seismol. Res. Lett. 80, 772–782, doi: 10.1785/gssrl.80.5.772.

Crowell, B. W., D. Melgar, Y. Bock, J. S. Haase, and J. Geng (2013). Earthquake magnitude scaling using seismogeodetic data, Geophys. Res. Lett. 40, 6089–6094.

Goldberg, D. E., D. Melgar, G. P. Hayes, B. W. Crowell, and V. J. Sahakian (2021). A ground motion model for GNSS peak ground displacement, Bull. Seismol. Soc. Am. 111, 2393–2407, doi: 10.1785/0120210042.

Hoechner, A., Ge, M., Babeyko, A. Y., and Sobolev, S. V.: Instant tsunami early warning based on real-time GPS – Tohoku 2011 case study, Nat. Hazards Earth Syst. Sci., 13, 1285–1292, https://doi.org/10.5194/nhess-13-1285-2013, 2013.

Melgar, D., Y. Bock, D. Sanchez, and B. W. Crowell (2013). On robust and reliable automated baseline corrections for strong motion seismology, J. Geophys. Res. 118, 1177–1187, doi: 10.1002/jgrb.50135.

Murray, J. R., B. W. Crowell, R. Grapenthin, K. Hodgkinson, J. O. Langbein, T. Melbourne, D. Melgar, S. E. Minson, and D. A. Schmidt (2018). Development of geodetic component for the U.S. West Coast earthquake early warning system, Seismol. Res. Lett. 89, 2322–2336, doi: 10.1785/0220180162.

Murray, J. R., B. W. Crowell, M. H. Murray, C. W. Ulberg, J. J. McGuire, M. A. Aranha, and M. T. Hagerty (2023). Incorporation of real-time earthquake magnitudes estimated via peak ground displacement scaling in the ShakeAlert earthquake early warning system, Bull. Seismol.

Sobolev, S. V., A. Y. Babeyko, R. Wang, A. Hoechner, R. Galas, M. Rothacher, D. V. Sein, J. Schröter, J. Lauterjung, and C. Subarya (2007), Tsunami early warning using GPS-Shield arrays, J. Geophys. Res., 112, B08415, doi:10.1029/2006JB004640.

Corresponding author: pietro.miele@ingv.it

Comparison of GNSS-derived geodetic strain rate estimates and seismicity rates in the Southern Apennines and Gargano area

P. Moretti[1], M. Massa[1], M. Filippucci[4], G. Selvaggi[3], A. Tallarico[4], G. Cecere[2]

[1] Istituto Nazionale di Geofisica e Vulcanologia (INGV), Sezione Milano

[2] Istituto Nazionale di Geofisica e Vulcanologia (INGV), Sezione Irpina

[3] Istituto Nazionale di Geofisica e Vulcanologia (INGV), Sezione Osservatorio Nazionale Terremoti

[4] Dipartimento di Scienze della Terra e Geoambientali, Università degli Studi di Bari "Aldo Moro" (UniBa), Bari, Italy

In the last decades, the development of permanent GNSS (Global Navigation Satellite System) networks has led to significant advances in the estimation of crustal deformation rates, providing fundamental insights into tectonic processes and seismic hazard assessment. However, the strain rate maps may vary substantially depending on the adopted methodology, the spatial heterogeneity of the GNSS stations and different data processing strategies. In this study, we analyze and compare three methods for estimating horizontal strain rate using the Strain_2D tool (Materna and Maurer, 2023), and evaluate their possible correlations with seismicity rates. These methods are applied to the Southern Apennine seismic belt and the Gargano promontory (Southern Italy), two areas characterized by complex and active tectonic deformation. We use a dense and updated GNSS velocity field derived from the analysis of observations from more than 100 permanent stations from multiple networks with time series lasting ≥ 4.5 years. GNSS displacements are estimated using the PRIDE PPP-AR (Precise Point Positioning with Ambiguity Resolution) (Geng et al., 2019) software, while velocity trends are derived through the MIDAS (Median Interannual Difference Adjusted for Skewness) (Blewitt et al., 2016) algorithm. An automated filtering procedure is then applied to identify and flag stations whose velocity vector are statistically inconsistent with those of neighboring stations, effectively removing outliers related to local instabilities or measurement errors (Piña-Valdés et al., 2022).

The strain rate estimation methods implemented in Strain_2D include: Nearest Neighbor approach, the VISR algorithm accounting for station density and spatial coverage, and a Wavelet-based multiscale method.

Preliminary results indicate that the estimated strain rate patterns show a non-negligible dependence on the adopted methodology, with differences in strain localization that may influence their spatial correspondence with observed seismicity rates. The analysis provides insights into the robustness and limitations of GNSS-based strain rate estimates for seismic hazard assessment.

References

Blewitt, Geoffrey, et al. "MIDAS robust trend estimator for accurate GPS station velocities without step detection." Journal of Geophysical Research: Solid Earth 121.3 (2016): 2054-2068

Geng, J., Chen, X., Pan, Y. et al. PRIDE PPP-AR: an open-source software for GPS PPP ambiguity resolution. GPS Solut 23, 91 (2019). https://doi.org/10.1007/s10291-019-0888-1

Materna K. and Maurer J., (2023). Quantification of geodetic strain rate uncertainties and implications for seismic hazard estimates, Geophys. J. Int., 234, 3, 2128-2142, doi: 10.1093/gji/ggad191

Materna K. and Maurer J., (2023). Strain_2D (version 1.1.1), url: https://code.usgs.gov/kmaterna/Strain_2D.%20 Archived%20at%20DOI:%2010. 5066/P9JJW0DY, https://github.com/kmaterna/Strain_2D

Piña-Valdés, J., A. Socquet, C. Beauval, M.-P. Doin, N. D'Agostino and Z.-K. Shen (2022). 3D GNSS velocity field sheds light on the deformation mechanisms in Europe: Effects of the vertical crustal motion on the distribution of seismicity, J. Geophys. Res.: Solid Earth, 127, https://doi.org/10.1029/2021JB023451

Corresponding author: pellegrino.moretti@ingv.it

An Integrated 3D Thermo-Rheological Model of the Southern Apennines (Italy): Insights from the TRHAM Project

M. Perrini[1,2], G. De Landro[2], G. Gola[3], F. Accomando[1], M. Fedi[4], V. Kastelic[5], P. Tizzani[1], D. Di Naccio[5], M. M. C. Carafa[5], G. Falcone[5], M. Taroni[5] and R. Castaldo[1]

Affiliations

1 Istituto per il Rilevamento Elettromagnetico dell'Ambiente (IREA), CNR, Naples, Italy
2 Dipartimento di Fisica "Ettore Pancini", Università degli Studi di Napoli, "Federico II", Naples, Italy
3 Istituto di Geoscienze e Georisorse (IGG), CNR, Turin, Italy
4 Dipartimento di Scienze della Terra (DiSTAR), Università degli Studi di Napoli "Federico II", Naples, Italy
5 Istituto Nazionale di Geofisica e Vulcanologia (INGV), L'Aquila, Italy

Abstract

Southern Italy is a tectonically active region of major geodynamic relevance, shaped by lithospheric convergence, crustal delamination, and long-lived fault systems associated with the eastward thrusting of formerly adjacent paleo-domains (e.g., Nicolai and Gambini, 2007; Patacca and Scandone, 2007). Consequently, the Southern Apennines constitute a highly heterogeneous crustal system, characterized by strong lateral and vertical variations in lithology, temperature, and fluid content. These heterogeneities exert a first-order control on crustal and upper-mantle rheology, influencing deformation styles, thermal evolution, and seismic behavior. In this study, we present the first regional-scale 3D thermo-rheological model of the Southern Apennines that integrates conductive and conductive-convective thermal regimes within a physically consistent crustal framework. The model builds upon the 3D geometric reconstruction developed within the TRHAM project ("Relation between 3D Thermo-Rheological Model and Seismic Hazard for Risk Mitigation in the Urban Areas of Southern Italy", funded under the PRIN2022 PNRR initiative by the European Union-Next Generation EU; Perrini et al., 2025) and results from a systematic synthesis and integration of multi-scale datasets across the Southern Apennines. These include direct wellbore and borehole information, regional and local geophysical observations (seismic tomography, gravity, and magnetic data), laboratory-derived P-wave velocity measurements for representative lithologies, and geological-structural syntheses from surface and subsurface data. Crustal architecture is reconstructed using a reproducible petrophysical methodology that links seismic velocities to lithological domains, enabling a physically consistent and internally coherent representation of the vertical and lateral structural organization of the crust (**Figure 1**).

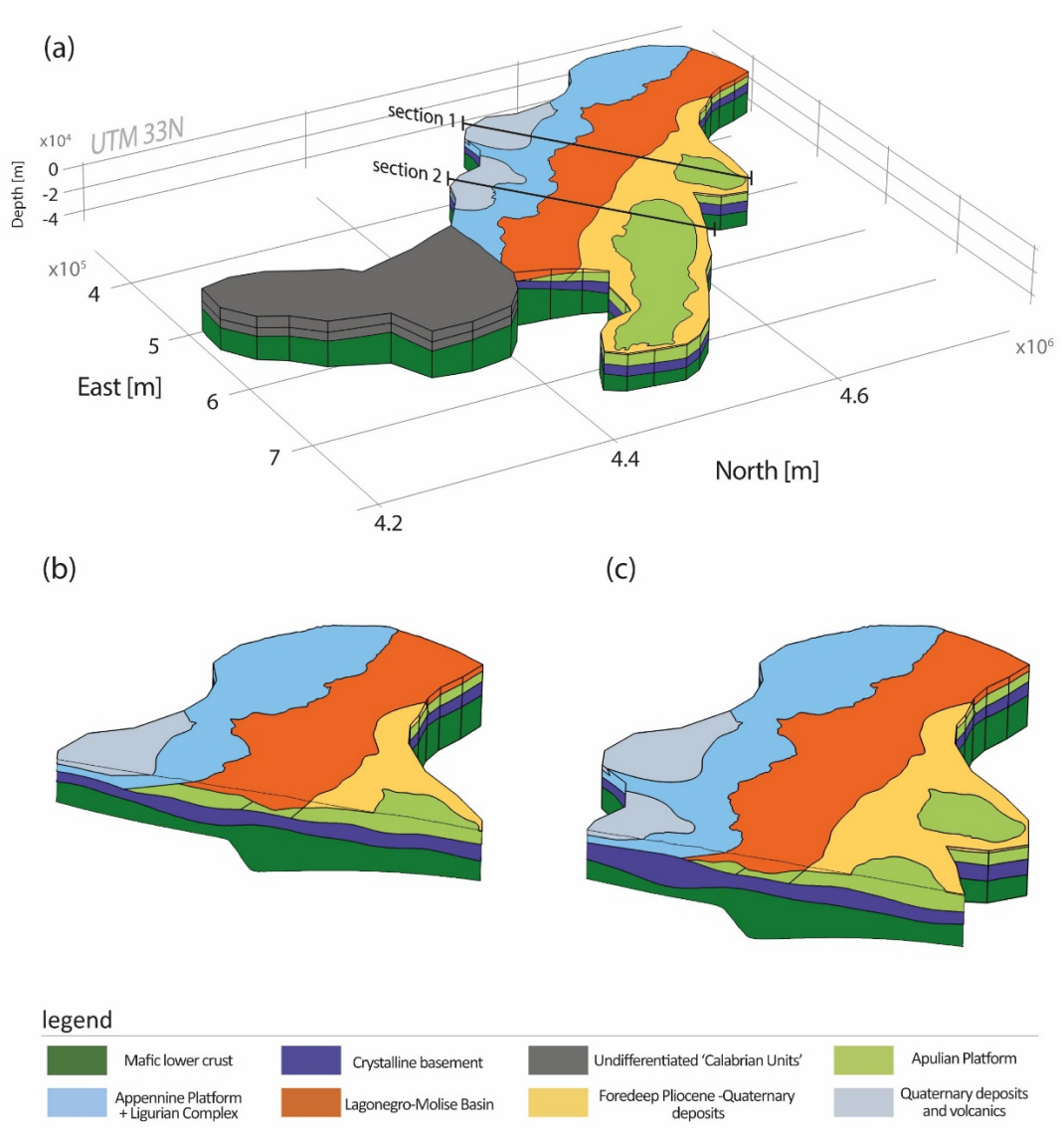

Figure 1 – 3D integrated crustal model of the Southern Apennines derived from the petrophysical methodology developed within the TRHAM Project. The model integrates geological, geophysical, and petrophysical constraints to reconstruct the crustal architecture and major lithological domains. In (a) overview of the finalized 3D model showing the traces of two reference cross-sections; (b) Section 1 - Campi Flegrei-Gargano transect; (c) Section 2 - CROP 04 profile. Further methodological details and interpretation are provided in Perrini et al. (2025).

The reconstructed geometry is discretized into a finite-element (FE) domain, where stationary conductive and coupled conductive-convective thermal regimes are simulated by solving the fully coupled system of Fourier heat conduction and Darcy flow equations in porous media. Thermo-hydro coupling is implemented through compaction- and temperature-dependent porosity and permeability laws, temperature-dependent thermal conductivity corrected following Sekiguchi et al. (1974), and internally generated radiogenic heat production following Lachenbruch (1970). Boundary conditions include an altitude-dependent temperature, a prescribed basal heat flow at Moho depth, and lateral adiabatic conditions. The resulting 3D convective thermal field provides the basis for thermo-rheological modeling; the crustal rheological transition are compared with the indipendent seismicity cutoff depth proposed by Chiarabba et al. (2025). Specifically, brittle deformation is described using a linear frictional failure law (Sibson, 1974), whereas ductile

behavior at elevated temperatures is modeled through power-law creep formulations (Kirby and Kronenberg, 1987). The model incorporates strain-rate estimates constrained by geodetic strain-rate maps, GNSS-derived frictional parameters representative of the prevailing kinematic regimes, and pore-fluid pressure ratios derived from convective thermal numerical modeling. This integrated approach enables quantification of the spatial variability of mechanical strength and fluid overpressure within a structurally heterogeneous and seismically active orogen. The computed strength envelopes highlight significant lateral variations in the depth, thickness, and geometry of the brittle-ductile transition across the Tyrrhenian-Adriatic transect. The explicit inclusion of fluid flow further highlights the key role of crustal geometry in controlling hydraulic connectivity and hydrological decoupling between the Apulian and Apenninic domains, which strongly modulates surface heat-flow patterns by focusing zones of fluid infiltration and discharge. This work represents the first comprehensive attempt to link three-dimensional crustal geometry, thermal state, fluid circulation, and mechanical behavior across the Southern Apennines. The proposed framework provides physically grounded constraints for geodynamic interpretation and establishes a robust foundation for regional-scale seismic hazard assessment within the TRHAM project.

Acknowledgments

This work is supported by the **TRHAM Project: Relation between 3D Thermo-Rheological Model and Seismic Hazard for Risk Mitigation in the Urban Areas of Southern Italy**, funded under the PRIN2022 PNRR initiative by the European Union-Next Generation EU.

References

Chiarabba, C., Menichelli, I., De Gori, P., & Lucente, F. P. (2025). Seismicity and deformation of the mobile continental lithosphere: An overview on the Alpine and Apennines orogens. *Earth-Science Reviews*, 271, 105299. https://doi.org/10.1016/j.earscirev.2025.105299

Kirby, S. H., & Kronenberg, A. K. (1987). Correction to "Rheology of the lithosphere: Selected topics." *Reviews of Geophysics*, 25(8), 1680–1681. https://doi.org/10.1029/RG025i008p01680

Lachenbruch, A. H. (1970). Crustal temperature and heat production: Implications of the linear heat-flow relation. *Journal of Geophysical Research*, 75(14), 2535–2549. https://doi.org/10.1029/JB075i014p02535

Nicolai, C., & Gambini, R. (2007). Structural architecture of the Adria platform-and-basin system. *Bollettino della Società Geologica Italiana*, 7, 21–37.

Patacca, E., & Scandone, P. (2007). Geological interpretation of the CROP-04 seismic line (Southern Apennines, Italy). *Italian Journal of Geosciences (Bollettino della Società Geologica Italiana)*, 7, 297–315.

Perrini, M., Accomando, F., De Landro, G., Gola, G., Tizzani, P., Carafa, M., Fedi, M., Zollo, A., Kastelic, V., Di Lorenzo, C., Di Naccio, D., Taroni, M., & Castaldo, R. (2025). An integrated 3D geological model of Southern Italy: Insights from the TRHAM Project. In *Proceedings of the 31st Meeting of Environmental and Engineering Geophysics (NSG 2025)*, European Association of Geoscientists and Engineers (EAGE), pp. 1–5.https://doi.org/10.3997/2214-4609.2025020267

Sibson, R. H. (1974). Frictional constraints on thrust, wrench and normal faults. *Nature*, 249, 542–544. https://doi.org/10.1038/249542a0

Corresponding author: perrini.m@irea.cnr.it

Numerical models of the post-collisional evolution of the southern Variscan belt: comparison with the Valpelline Series (western Alps)

A. Regorda[1], M. Filippi[1], M. Roda[1]

[1] *Università degli Studi di Milano, Milan, Italy*

The Wilson Cycle is a fundamental framework for understanding Earth's long-term geological evolution, yet the transition from continental collision to post-orogenic extension and eventual final break-up remains poorly constrained. This stage is particularly difficult to investigate because deep crustal rocks commonly experience multiple tectono-metamorphic overprints during exhumation, overprinting earlier records. Additional challenges arise from uncertainties in Pressure-Temperature (PT) estimates and metamorphic geochronology, which complicate the discrimination of successive events along a single exhumation path.

The Variscan remnants preserved within the Alpine chain represent an exceptional natural laboratory to explore these processes. In fact, in the Alps, deep Variscan crust was exhumed during the Alpine cycle, retaining evidence of Devonian-Carboniferous subduction and collision related to Variscan convergence (Roda et al., 2023, and references therein). This convergent history was followed in the early Permian by widespread high- to ultra-high-temperature metamorphism and gabbroic magmatism (e.g., Schuster and Stüwe, 2008), interpreted as the expression of a large-scale transtensional regime linked to early Permian shear zones active across Pangea (Muttoni et al., 2003).

In this study, we investigate the thermo-mechanical evolution of convergent-divergent tectonic systems using the 2D numerical code FALCON (Regorda et al., 2023), with particular emphasis on post-collisional processes. In particular, we developed three models: 1) a model characterised by instantaneous extension after collision (EMod); 2) a model characterised by a pure gravitational phase of 5 Myr before the extensione (GMod5) and; 3) a model with an intermediate phase of pure gravitational evolution lasting 10 Myr (GMod10). Pressure-Temperature-time (PTt) paths predicted by the models are then compared with geological constraints from Permian granulite-facies rocks of the Valpelline Series (Western Alps), where two distinct metamorphic stages have been identified (M1 and M2).

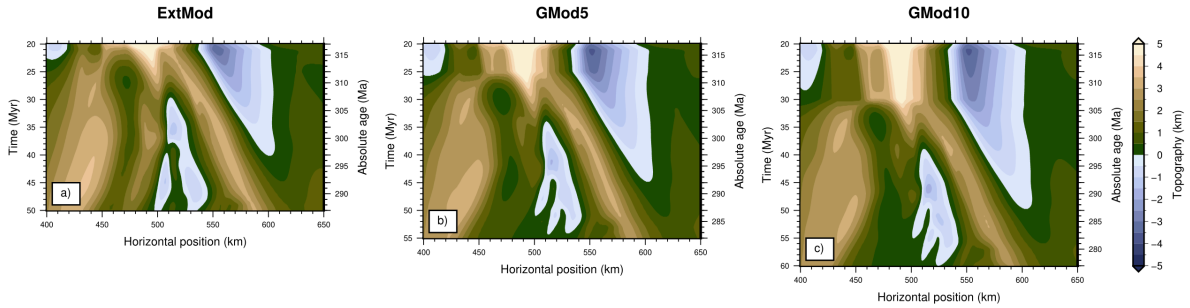

Fig. 1 - Post-collisional topography evolution for models EMod (panel a), GMod5 (panel b) and GMod10 (panel c).

Our simulations show that the onset of post-collisional divergence promotes the reactivation of structures inherited from the preceding convergence phase. Strain localizes preferentially along the former subduction channel, while extension in the upper crust is accommodated by normal faulting that re-activates pre-existing inverse structures. This evolution leads to progressive thinning of the overthickened continental crust, driven by asthenospheric upwelling beneath the slab. This process is favoured by the relatively high temperatures and low viscosities at the base of the subducting plate with respect to the mantle wedge, leading to efficient strain localization. Concurrently, surface topography decreases, with the development of shallow sedimentary basin (maximum 1000-1500 m; Fig. 1) consistent with early Permian basins observed in the Southern Alps (Cassinis and Perotti, 2007).

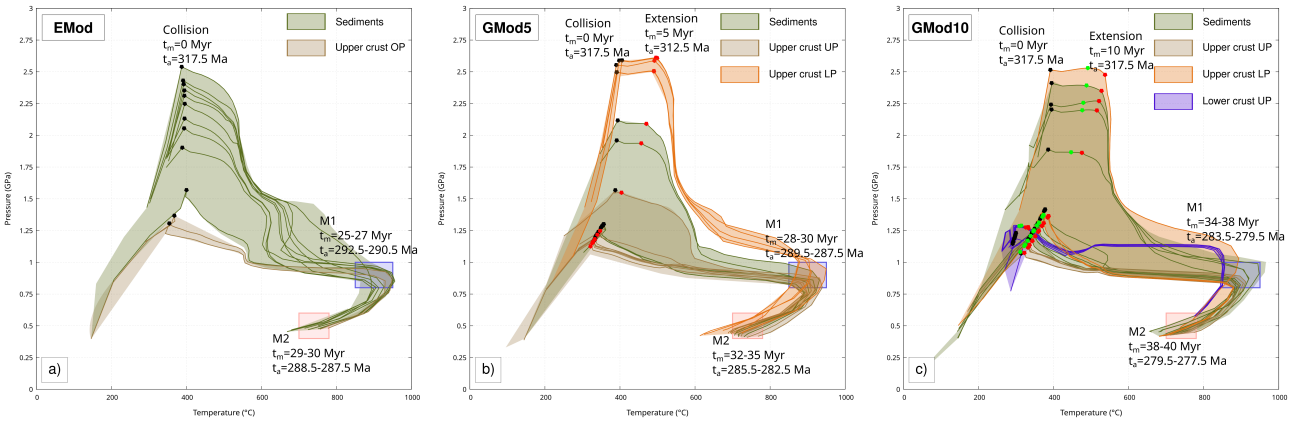

Fig. 2 - PT paths of markers of EMod (panel a), GMod5 (panel b) and GMod10 (panel c) models fitting with M1 and M2. The green area represents the paths of sediments, the brown area represents the paths of upper continental markers of the upper plate, the light brown area represents the paths of of upper continental markers of the lower plate, while the blue area represents the paths of the lower continental markers of the upper plate. Green, brown, light brown and blue lines are some example of PT paths predicted by the model. Black dots indicate the PT conditions at the continental collision; red dots in panels b and c indicate the PT conditions at the beginning of the extension; the green dots in panel c indicate the PT conditions after 5 Myr of gravitational phase for the GMod10 model. Rectangles indicate the PT conditions compatible with M1 (blue) and M2 (pink).

The PTt paths predicted for sedimentary and continental crustal markers display a maximum pressure at the continental collision (black dots in Fig. 2), followed by exhumation associated with heating. The thermal peak is then reached during the first metamorphic event (M1) recorded in the Valpelline Series at 297–291 Ma (blue rectangles in Fig. 2). The following exhumation is marked

by cooling, reproducing the conditions of a second metamorphic event (M2) documented at 290-284 Ma (pink rectangles in Fig. 2). The agreement between model results and natural PT estimates suggests that the initiation of a divergent tectonic regime shortly after collision (maximum 5 Myr) is required to explain the observed metamorphic evolution. Conversely, a simple gravitational collapse do to reproduce the high-temperature PT history, implying the need to reassess the tectonic framework of the late Carboniferous-early Permian and questioning the traditional role attributed to gravitational collapse in classical Wilson Cycle models.

References

G. Cassinis and C. Perotti; 2007: A stratigraphic and tectonic review of the italian southern alpine permian. Palaeoworld, 16(1):140–172, doi:10.1016/j.palwor.2007.05.004. Contributions to Permian and Carboniferous Stratigraphy, Brachiopod Palaeontology and End-Permian Mass Extinctions, In Memory of Professor Yu-Gan Jin.

G. Muttoni, D. V. Kent, E. Garzanti, P. Brack, N. Abrahamsen, and M. Gaetani; 2003: Early permian pangea 'b' to late permian pangea 'a'. Earth and Planetary Science Letters, 215(3):379–394, doi:10.1016/S0012-821X(03)00452-7.

A. Regorda, C. Thieulot, I. van Zelst, Z. Erdős, J. Maia, and S. Buiter. Rifting venus: Insights from numerical modeling; 2023: Journal of Geophysical Research: Planets, 128(3), e2022JE007588, doi:10.1029/2022JE007588.

M. Roda, M. I. Spalla, M. Filippi, J.-M. Lardeaux, G. Rebay, A. Regorda, D. Zanoni, M. Zucali, and G. Gosso; 2023: Metamorphic Remnants of the Variscan Orogeny across the Alps and Their Tectonic Significance. Geosciences, 10(13):300, doi:10.3390/geosciences13100300.

R. Schuster and K. Stüwe; 2008: Permian metamorphic event in the Alps. Geology, 36:603–606, doi:10.1130/G24703A.1.

Corresponding author: alessandro.regorda@unimi.it

Integrated seismic–gravity model of the Southern Apennines

R. Tondi[1], C. Piromallo[2], P. De Gori[3], L. Improta[3], F. Di Luccio[2]

[1] Istituto Nazionale di Geofisica e Vulcanologia – Sezione di Bologna – Bologna, Italy
[2] Istituto Nazionale di Geofisica e Vulcanologia – Sezione di ROMA1 – Rome, Italy
[3] Istituto Nazionale di Geofisica e Vulcanologia – ONT – Rome, Italy

1. Introduction and Geological Motivation

The Southern Apennines represent one of the most complex and actively deforming sectors of the Mediterranean orogenic system. Their present-day architecture results from the long-term interaction between the convergence of the Adria plate and the rollback of the Ionian slab, coupled with back-arc extension in the Tyrrhenian domain. This geodynamic setting produces a pronounced lateral and vertical heterogeneity of the crust and upper mantle, reflected in seismicity patterns, heat flow anomalies, active degassing, and strong gravity signals. Despite decades of investigation, the deep structure of the Southern Apennines remains only partially constrained, particularly at lower-crustal depths.

Instrumental seismicity in the Apennines is mainly confined to the upper ~15 km and shows a characteristic East–West elongation, reflecting the regional extensional stress regime. As a consequence, seismic tomography alone provides limited resolution of deeper crustal volumes, where ray coverage rapidly decreases and velocity anomalies become more difficult to interpret unambiguously. This limitation has hindered the resolution of several long-debated questions, including the role of the crystalline basement in deformation, the geometry of the Adria plate at depth, and the possible presence of slab tears or lithospheric discontinuities beneath the chain.

To overcome these limitations, we developed a three-dimensional model of the upper and lower crust of the Southern Apennines by integrating seismic tomography and gravity data within the SII framework (Tondi et al., 2012). The seismic component is based on the velocity model of Improta et al. (2014), which provides a robust reference framework for the region and allows for the calibration of optimization parameters specific to the Southern Apennines. Gravity constraints are introduced through a Bouguer anomaly dataset (Fig. 1) covering the entire Mediterranean area, including both continental and offshore measurements, ensuring homogeneous regional coverage and consistent boundary conditions. The integration of these complementary datasets enables us to improve model resolution at depth and to reduce non-uniqueness in the interpretation of crustal density and velocity variations.

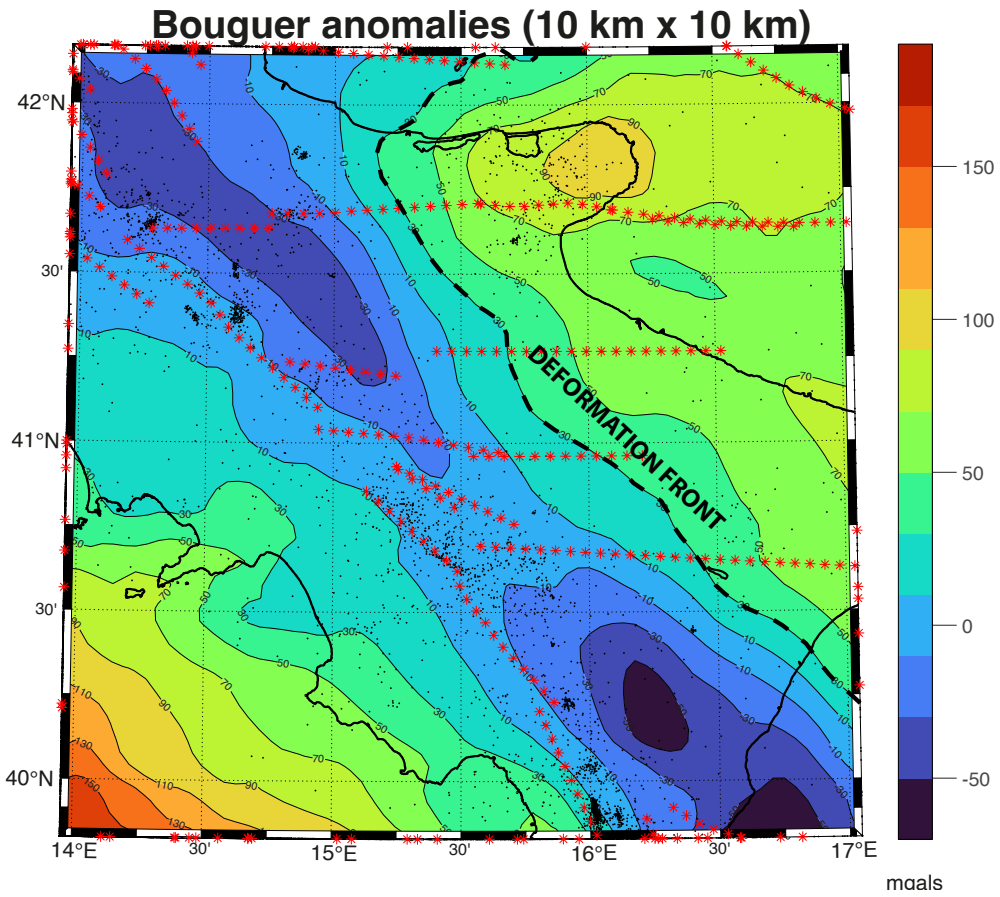

***Figure 1**. Bouguer anomaly map of the Southern Apennines derived from the Mediterranean gravity dataset (ISPRA, ENI, OGS, 2009; scale 1:250,000). Earthquake hypocenters (black dots) for seismicity with magnitude M > 2, major seismogenic faults (red stars), and the deformation front are shown for reference.*

2. Integrated model results: horizontal and vertical sections

The integrated seismic–gravity model is analyzed through a set of horizontal slices and vertical cross sections and is systematically compared with the seismic tomography model alone. This comparison highlights the added value of gravity constraints, particularly in terms of resolved volume and continuity of anomalies at lower-crustal depths.

Horizontal sections (Fig. 2) show that the integrated model provides a clearer and more coherent definition of crustal structures, especially below ~20 km depth. In several areas, velocity and density anomalies that appear diffuse or poorly constrained in the seismic-only model become sharper and laterally more continuous when gravity data are included. This improvement is particularly evident in the Lucanian Arc, where the curvature of the chain is associated with strong lateral variations in basement properties. Here, the integrated model reveals a pronounced heterogeneity of the crustal basement, suggesting its active involvement in deformation processes. These observations support a thick-skinned tectonic style, at least locally, in which deformation affects not only the sedimentary cover but also the underlying crystalline basement of the Apulian platform.

At greater depths, the model highlights rigid, high-density and high-velocity bodies that we interpret as fragments of the Adria plate. These bodies are embedded within a lower crust characterized by reduced velocities and densities, consistent with elevated temperatures and possibly partial melting. This thermal and rheological contrast is interpreted as the deep expression of the extensional regime associated with the Tyrrhenian back-arc basin. The spatial distribution of these

anomalies suggests a strong coupling between slab dynamics, back-arc extension, and crustal-scale deformation in the Southern Apennines.

Between approximately 26 and 34 km depth, a prominent anomaly is identified that disrupts the continuity of the interpreted Adria plate. We interpret this feature as a possible tear or major discontinuity within the subducting lithosphere. Such a tear could facilitate localized mantle upwelling and may be responsible for observed rotations of crustal blocks and changes in structural trends along the chain. This interpretation is consistent with regional geodynamic models invoking slab segmentation to explain the complex kinematics of the Apennine system.

Vertical cross sections (Fig. 3) crossing areas affected by strong thermal anomalies and intense CO_2 emissions provide further insights into crust–mantle interactions. In these sections, a positive correlation is observed between Bouguer gravity anomalies and topography. This relationship is not compatible with simple isostatic compensation, which would predict an anticorrelation between relief and density. Instead, the observed pattern suggests the presence of dense mantle-derived material or fluids rising into the lower crust.

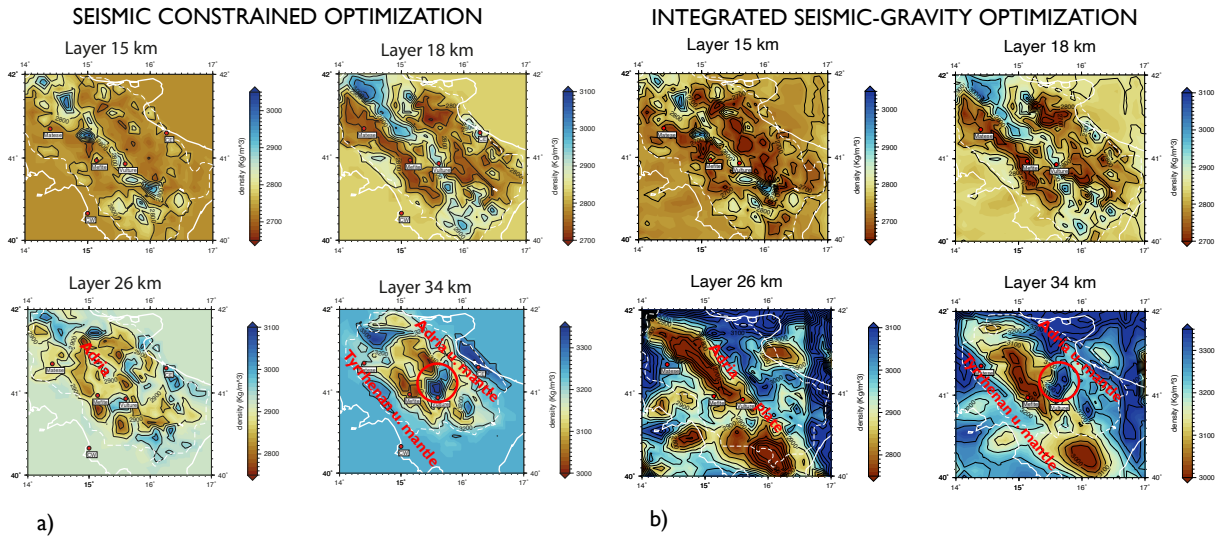

Figure 2. Comparison between horizontal slices of the seismic tomography model (a) and the integrated seismic–gravity model (b) at selected depths. The integrated model shows improved resolution and continuity of anomalies, particularly in the lower crust.

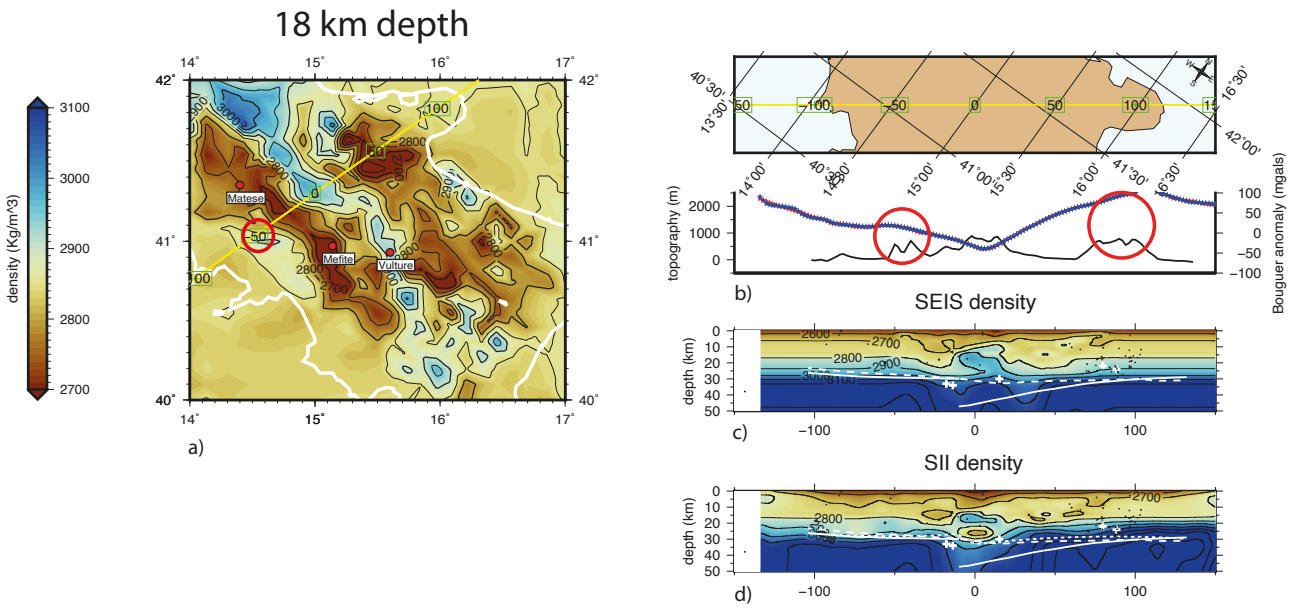

Figure 3. *Representative vertical cross sections across a thermally anomalous area of the Southern Apennines, whose location is shown in panel (a). Panel (b) illustrates the positive correlation between Bouguer anomalies and topography. Panels (c) and (d) show cross sections through the seismic model and the SII model, respectively, together with Moho depths derived from different models: Spada et al. (2009; white continuous line), EPCrust (Molinari et al., 2011; white dashed line), Di Stefano and Ciaccio (2014; white long-dashed line), and Piana Agostinetti (2009; crosses). Seismicity is indicated by black dots.*

3. Geodynamic Implications and Conclusions

The integrated seismic–gravity model presented here provides a refined image of the lower crust beneath the Southern Apennines and offers new constraints on long-standing geodynamic problems. The results support a tectonic scenario in which thick-skinned deformation plays a significant role, particularly in structurally complex sectors such as the Lucanian Arc. This finding has important implications for the mechanical behavior of the Apennine belt and for the interpretation of surface structures in terms of deep processes.

The identification of rigid Adria plate fragments surrounded by a warmer, weaker lower crust emphasizes the importance of thermal and rheological heterogeneities in controlling deformation. The inferred tear in the subducting Adria plate represents a key feature that may link deep mantle dynamics to surface tectonics, providing a pathway for mantle upwelling and influencing the distribution of seismicity, magmatism, and fluid flow.

The observed positive correlation between Bouguer anomalies and topography in areas characterized by high heat flow and CO_2 emissions further supports a model involving mantle-derived fluids or hot material rising into the crust. Such processes can generate positive mass anomalies and regional uplift, while simultaneously affecting the stress state of the crust and potentially contributing to seismic hazard.

Overall, this study demonstrates the effectiveness of integrating seismic tomography and gravity data to improve imaging of deep crustal structures in regions where seismic resolution alone is insufficient. This integrated approach provides a valuable basis for future investigations into the

geodynamics, seismicity, and fluid circulation of the Southern Apennines and comparable orogenic systems worldwide.

References

R. Di Stefano, M. G. Ciaccio; 2014: The lithosphere and asthenosphere system in Italy as inferred from the Vp and Vs 3D velocity model and Moho map. Journal of Geodynamics, doi: 10.1016/j.jog.2014.09.006

L. Improta, P. De Gori, C. Chiarabba; 2014: New Insights into crustal structure, Cenozoic magmatism, CO_2 degassing, and seismogenesis in the southern Apennines and Irpinia region from local earthquake tomography. JGR – Solid Earth, doi:10.1002/2013JB010890.

Molinari I., A. Morelli; 2011: EPcrust: a reference crustal model for the European Plate. JGI, doi: 10.1111/j.1365-246X.2011.04940.x

N. Piana Agostinetti, A. Amato; 2009: Moho depth and Vp/Vs ratio in peninsular Italy from teleseismic receiver functions. JGR – Solid Earth, doi: 10.1029/2008JB005899.

R. Tondi, C. Cavazzoni, P. Danecek, A. Morelli; 2012: Parallel, 'large', dense matrix problems: Application to sequential integrated inversion of seismological and gravity data. Computers and Geosciences, doi: 10.1016/j.cageo.2012.05.026.

Corresponding author: rosaria.tondi@ingv.it